Acid sphingomyelinase modulates the autophagic process by controlling lysosomal biogenesis in Alzheimer's disease

Jong Kil Lee,[1,2,3] Hee Kyung Jin,[1,4] Min Hee Park,[1,2,3] Bo-ra Kim,[1,2,3] Phil Hyu Lee,[5] Hiromitsu Nakauchi,[6] Janet E. Carter,[7] Xingxuan He,[8] Edward H. Schuchman,[8] and Jae-sung Bae[1,2,3]

[1]Stem Cell Neuroplasticity Research Group, [2]Department of Physiology, Cell and Matrix Research Institute, School of Medicine, [3]Department of Biomedical Science, BK21 Plus KNU Biomedical Convergence Program, [4]Department of Laboratory Animal Medicine, College of Veterinary Medicine, Kyungpook National University, Daegu 702-701, Korea
[5]Department of Neurology and Brain Research Institute, Yonsei University College of Medicine, Seoul 120-752, Korea
[6]Division of Stem Cell Therapy, Center for Stem Cell Biology and Regenerative Medicine, Institute of Medical Science, University of Tokyo, Tokyo 108-8639, Japan
[7]Mental Health Sciences Unit, Faculty of Brain Sciences, University College London, London WC1E 6DE, England, UK
[8]Department of Genetics and Genomic Sciences, Icahn School of Medicine at Mount Sinai, New York, NY 10029

In Alzheimer's disease (AD), abnormal sphingolipid metabolism has been reported, although the pathogenic consequences of these changes have not been fully characterized. We show that acid sphingomyelinase (ASM) is increased in fibroblasts, brain, and/or plasma from patients with AD and in AD mice, leading to defective autophagic degradation due to lysosomal depletion. Partial genetic inhibition of ASM (*ASM*$^{+/-}$) in a mouse model of familial AD (FAD; *amyloid precursor protein* [*APP*]*/presenilin 1* [*PS1*]) ameliorated the autophagocytic defect by restoring lysosomal biogenesis, resulting in improved AD clinical and pathological findings, including reduction of amyloid-β (Aβ) deposition and improvement of memory impairment. Similar effects were noted after pharmacologic restoration of ASM to the normal range in APP/PS1 mice. Autophagic dysfunction in neurons derived from FAD patient induced pluripotent stem cells (iPSCs) was restored by partial ASM inhibition. Overall, these results reveal a novel mechanism of ASM pathogenesis in AD that leads to defective autophagy due to impaired lysosomal biogenesis and suggests that partial ASM inhibition is a potential new therapeutic intervention for the disease.

CORRESPONDENCE
Jae-sung Bae:
jsbae@knu.ac.kr

Abbreviations used: Aβ, amyloid-β; AC, acid ceramidase; AD, Alzheimer's disease; ALP, autophagy–lysosome pathway; AMI, amitriptyline-hydrochloride; AP, alkaline phosphatase; ApoE4, apolipoprotein E4; APP, amyloid precursor protein; ASM, acid sphingomyelinase; AV, autophagic vacuole; CM, conditioned medium; EM, electron microscope; FAD, familial AD; i.c., intracerebral; iPSC, induced pluripotent stem cell; Lamp1, lysosomal-associated membrane protein 1; LBPA, lysobisphosphatidic acid; LC3, microtubule-associated protein 1 light chain 3; M6P, mannose-6-phosphate; NPD, Niemann-Pick disease; PD, Parkinson's disease; PS1, presenilin 1; SA-β-gal, senescence-associated-β-galactosidase; TFEB, transcription factor EB.

Alzheimer's disease (AD) is the most common form of dementia. It is characterized clinically by progressive loss of memory, and pathologically by the presence of neuritic plaques and neurofibrillary tangles (Selkoe, 2001). There are profound biochemical alterations in multiple pathways in the AD brain, including changes in amyloid-β (Aβ) metabolism, tau phosphorylation, and lipid regulation, although to date the underlying mechanisms leading to these complex abnormalities, as well as the downstream consequences, remain largely unknown (Yankner et al., 2008; He et al., 2010; Mielke et al., 2012).

Sphingolipid metabolism is an important process for tissue homeostasis that regulates the formation of several bioactive lipids and second messengers that are critical in cellular signaling (Lahiri and Futerman, 2007; Wymann and Schneiter, 2008). In the brain, the proper balance of sphingolipid metabolites is essential for normal neuronal function, and subtle changes in sphingolipid homeostasis may be intimately involved in neurodegenerative diseases including AD (Cutler et al., 2004; Grimm et al., 2005; Hartmann et al., 2007; Grösgen et al., 2010; Haughey et al., 2010; Mielke and Lyketsos, 2010; Di Paolo and Kim, 2011; Tamboli et al., 2011).

Recently, our studies and those of others (Katsel et al., 2007; He et al., 2010) have shown that the activity of several sphingolipid metabolizing enzymes, including acid sphingomyelinase

J.K. Lee and H.K. Jin contributed equally to this paper.

The Rockefeller University Press $30.00
J. Exp. Med. 2014 Vol. 211 No. 8 1551-1570
www.jem.org/cgi/doi/10.1084/jem.20132451

The Journal of Experimental Medicine

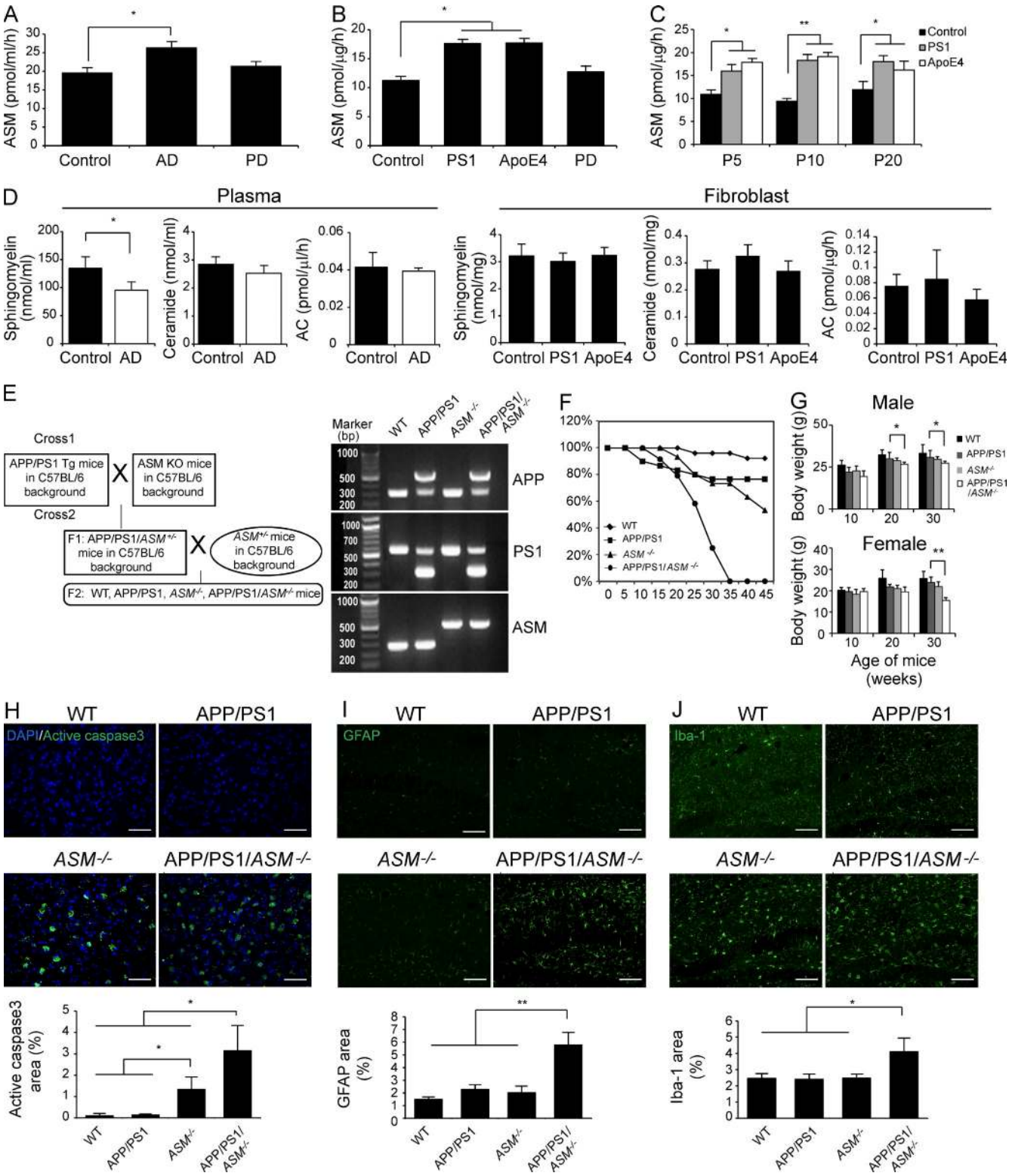

Figure 1. ASM is increased in AD and complete ASM gene deficiency exacerbates pathology of APP/PS1 mice. (A and B) ASM was estimated in the blood plasma (A; control, $n = 30$; AD, $n = 40$; and PD, $n = 20$) and fibroblast (B; control, $n = 24$; PS1-FAD, $n = 24$; ApoE4, $n = 24$; and PD, $n = 12$) with AD, PD, or normal controls. (C) ASM activity did not show passage differences between AD and normal fibroblasts ($n = 8$ per passage group). (D) Detection of sphingomyelin, ceramide, and AC in plasma (control, $n = 20$–22; and AD, $n = 33$–35) and fibroblast (control, $n = 12$; PS1-FAD, $n = 18$; and ApoE4, $n = 18$). (E) Crossing scheme to generate WT, APP/PS1, $ASM^{-/-}$, and APP/PS1/$ASM^{-/-}$ mice. PCR-based genotyping to detect WT, APP/PS1, $ASM^{-/-}$, and APP/PS1/$ASM^{-/-}$ mice. (F) Survival curves of WT ($n = 26$), APP/PS1 ($n = 30$), $ASM^{-/-}$ ($n = 30$), and APP/PS1/$ASM^{-/-}$ ($n = 25$) mice. (G) Body weights of WT,

(ASM), are abnormal in the brains of AD patients. ASM is expressed by almost all cell types and has an important housekeeping role in sphingolipid metabolism and membrane turnover. It is mainly located within the endosomal/lysosomal compartment but is associated with the cellular stress response and may become preferentially transported to the outer leaflet of the cell membrane under conditions of cell stress (Jenkins et al., 2009). Mutations in the ASM gene (*SMPD1*) lead to the type A and B forms of the lysosomal storage disorder Niemann-Pick disease (NPD). In addition to its role in NPD, the importance of ASM in numerous signaling processes, including cell death, inflammation, and autophagy, has been extensively documented in several pathological conditions (Santana et al., 1996; Górska et al., 2003; Petrache et al., 2005; Lang et al., 2007; Smith and Schuchman, 2008; Teichgräber et al., 2008; Sentelle et al., 2012). However, the role of ASM in AD and the cellular mechanisms that link ASM and AD have not been fully characterized. This lack of understanding between the correlation of altered ASM levels and AD pathophysiology led us to explore the mechanisms underlying ASM's role in AD pathogenesis. Here, we show for the first time that increased ASM activity in AD causes a defect of autophagic degradation due to disruption of lysosomal biogenesis and integrity, and that partial inhibition of ASM activity leads to restoration of autophagy and improvement of pathological and clinical findings in AD mice.

RESULTS

ASM activity is increased in AD patients

We first sought to confirm whether sphingolipid metabolism is altered in AD patient samples. We examined ASM and acid ceramidase (AC) activities, and the levels of several sphingolipids, including sphingomyelin and ceramide, in samples from normal individuals and AD patients. Consistent with previous results (He et al., 2010), ASM was significantly increased in plasma and fibroblasts from individuals with AD compared with normal aged individuals (Fig. 1, A and B). To assess whether increased ASM activity was an AD-specific signature, we analyzed ASM activity in samples from individuals with Parkinson's disease (PD). The activity of ASM was not elevated in PD-derived samples compared with normal (Fig. 1, A and B). ASM activity also did not show passage differences between AD and normal fibroblasts (Fig. 1 C). Sphingomyelin levels were decreased in the AD plasma compared with normal (Fig. 1 D). No significant differences in the ceramide and AC levels were found between the two groups (Fig. 1 D). These results confirmed that elevation of ASM, an important sphingolipid-modulating factor, is AD specific and may influence disease progression and/or pathogenesis.

Partial ASM inhibition in AD mice reduces pathology

To investigate the influence of ASM on AD pathology, we first generated amyloid precursor protein (APP)/presenilin 1 (PS1) double mutant and APP/PS1/$ASM^{-/-}$ triple mutant mice (Fig. 1 E). AD-related pathologies in APP/PS1 mice normally begin at ∼6–7 mo of age; however, our APP/PS1/$ASM^{-/-}$ mice died young (Fig. 1 F). We presume that the early death of the APP/PS1/$ASM^{-/-}$ animals was due to their $ASM^{-/-}$ phenotype because these animals (originally developed as a model of the neurodegenerative type A NPD) usually die by ∼6–8 mo of age. The APP/PS1/$ASM^{-/-}$ mice showed significantly decreased body weight compared with APP/PS1 mice (Fig. 1 G), and indicators of brain injury, such as cell death and inflammation, were significantly increased (Fig. 1, H–J). These data demonstrated that complete deletion of ASM in APP/PS1 mice exacerbated brain pathology, and that APP/PS1/$ASM^{-/-}$ mice were not suitable to examine the correlation of ASM and AD pathology.

To overcome these obstacles, we generated APP/PS1/$ASM^{+/-}$ triple mutant mice (with partial genetic deletion of the ASM gene; Fig. 2, A and B). Similar to AD patients, ASM activity was elevated in plasma, brain, and fibroblasts of 9-mo-old APP/PS1 mice (Fig. 2 C), likely due to the stress response related to the progression of AD-like disease in these animals. Next, to further investigate the cell contribution of increased ASM activity in AD mouse brain, we isolated neurons and microglia from the brain. Although ASM activity was slightly increased in APP/PS1 microglia compared with WT microglia, the degree of ASM increase was greater in neurons than microglia (Fig. 2 D), indicating that neurons were the main contributor of elevated ASM activity in AD mouse brain.

Importantly, ASM activity in age-matched APP/PS1/$ASM^{+/-}$ mice was significantly decreased compared with the APP/PS1 mice to levels within the normal range or lower (Fig. 2 C). Other sphingolipid factors were unaltered in the APP/PS1/$ASM^{+/-}$ mice except sphingomyelin, which was modestly reduced in APP/PS1 mice and elevated in the triple mutant animals (Fig. 2 E).

To determine whether the reduced ASM activity in the APP/PS1/$ASM^{+/-}$ mice affected AD pathology, we first determined the Aβ profile. Thioflavin S staining, immunofluorescence, and ELISA results of Aβ40 and Aβ42 showed significantly lower Aβ levels in the 9-mo-old APP/PS1/$ASM^{+/-}$ mice compared with age-matched APP/PS1 mice (Fig. 2, F–I). In APP/PS1/$ASM^{+/-}$ mice, cerebral amyloid angiopathy and C-terminal fragment of APP were also reduced (Fig. 2 J; and see Fig. 4, D and F). There were no significant differences of tau hyperphosphorylation between the two groups (Fig. 2 K).

APP/PS1, $ASM^{-/-}$, and APP/PS1/$ASM^{-/-}$ mice were determined at the indicated ages (n = 6–7 per group). (H–J) Brain sections from 7-mo-old mice were immunostained with anti–active caspase3 (H; n = 4 per group; bars, 50 µm), anti-GFAP (I; n = 4 per group; bars, 100 µm), and anti–Iba-1 (J; n = 4 per group; bars, 100 µm). Data are representative of three independent experiments. A–D and G, Student's t test. H–J, one-way ANOVA, Tukey's post hoc test. *, $P < 0.05$; **, $P < 0.01$. All error bars indicate SEM.

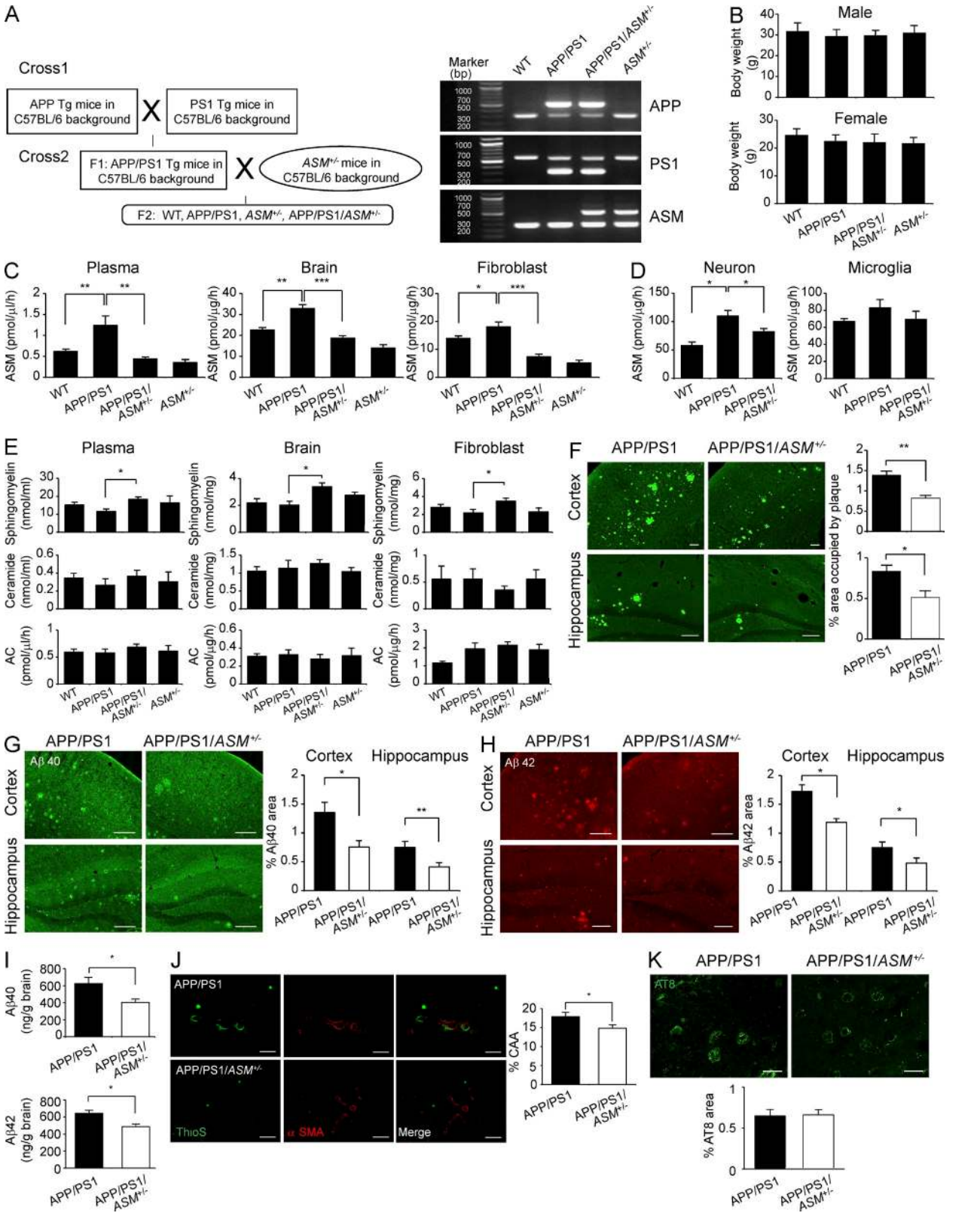

Figure 2. Partial genetic inhibition of ASM leads to decreased AD pathology in the APP/PS1 mice. (A) Generation of the APP/PS1/*ASM*$^{+/-}$ mice. (B) Body weights of WT, APP/PS1, *ASM*$^{+/-}$, and APP/PS1/*ASM*$^{+/-}$ mice were determined at 9 mo of age (n = 14 per group). (C) ASM activity in blood plasma (n = 14–15 per group), brain (n = 13–14 per group), and fibroblast (n = 8 per group) derived from WT, APP/PS1, *ASM*$^{+/-}$, and APP/PS1/*ASM*$^{+/-}$ mice. (D) ASM activity was assessed in neuron and microglia isolated from mouse brain (WT, n = 8; APP/PS1, n = 6; and APP/PS1/*ASM*$^{+/-}$, n = 6). (E) Detection of sphingomyelin, ceramide, and AC in

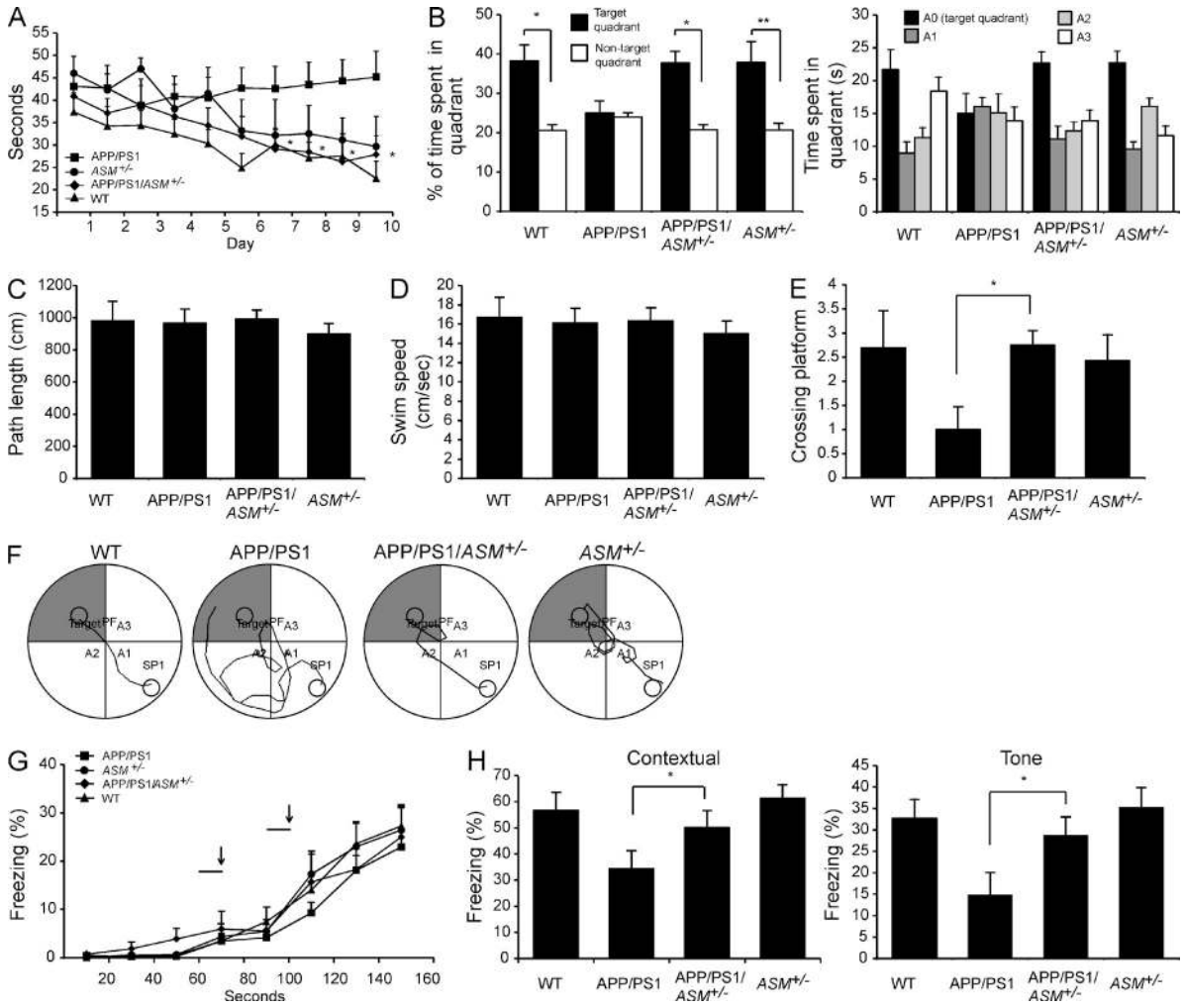

Figure 3. Partial genetic inhibition of ASM prevents memory impairments in APP/PS1 mice. (A) Learning and memory was assessed by Morris water maze test in the WT (n = 13), APP/PS1 (n = 12), $ASM^{+/-}$ (n = 12), and APP/PS1/$ASM^{+/-}$ (n = 12) mice (B–F) Probe trial day 11. (B) Time spent in target platform and other quadrants was measured. (C and D) Path length (C) and swim speed (D) were analyzed. (E) The number of times each animal entered the small target zone during the 60-s probe trial. (F) Representative swimming paths at day 10 of training. (G) The freezing response during the training session. Bars show exposure to the tone and arrows the application of the footshock. (H) The results of contextual and tone tasks (WT, n = 14; APP/PS1, n = 14; $ASM^{+/-}$, n = 13; and APP/PS1/$ASM^{+/-}$, n = 13). Data are representative of three independent experiments. A, C, D, E, and H, one-way ANOVA, Tukey's post hoc test. B, Student's t test. *, $P < 0.05$; **, $P < 0.01$. All error bars indicate SEM.

Next, to assess the potential effect of partial genetic ASM inhibition on learning and memory in APP/PS1 mice, we performed the Morris water maze task and fear conditioning. Aged APP/PS1 mice showed severe deficits in memory formation and APP/PS1/$ASM^{+/-}$ mice were largely protected from this defect (Fig. 3). Collectively, these results suggested that restored ASM activities to the normal range in APP/PS1 mice decreased Aβ load and improved learning and memory.

Partial ASM inhibition reverses defective autophagy in AD mice

A reduction in APP/PS1/$ASM^{+/-}$ mouse cerebral amyloidosis could be due to a decreased inflammatory response, attenuated APP expression, or activation of proteases involved in Aβ degradation. We first assessed the apoptotic and inflammatory responses in brain samples derived from APP/PS1 and APP/PS1/$ASM^{+/-}$ mice but did not detect differences between

plasma (n = 8–10 per group), brain (n = 7–9 per group), and tail (n = 5–6 per group) fibroblast. (F) Mice brain sections were stained with thioflavin S in APP/PS1 and APP/PS1/$ASM^{+/-}$ mice. The relative area occupied by Aβ plaques were determined (n = 6–7 per group; bars, 100 µm). (G–I) Analysis of Aβ40 and Aβ42 depositions from the mice brain samples using immunofluorescence staining (G and H; n = 6–7 per group; bars, 200 µm) and ELISA kits (I; n = 8 per group). (J and K) Confocal laser microscope images and quantification of cerebral amyloid angiopathy (J; n = 6 per group; bars, 50 µm) and tau hyperphosphorylation (K; n = 6 per group; bars, 20 µm) in APP/PS1 and APP/PS1/$ASM^{+/-}$ mice. Data are representative of two (D and K), three (B, C, and E), or four (F–J) independent experiments. B–E, one-way ANOVA, Tukey's post hoc test. F–K, Student's t test. *, $P < 0.05$; **, $P < 0.01$; ***, $P < 0.005$. All error bars indicate SEM.

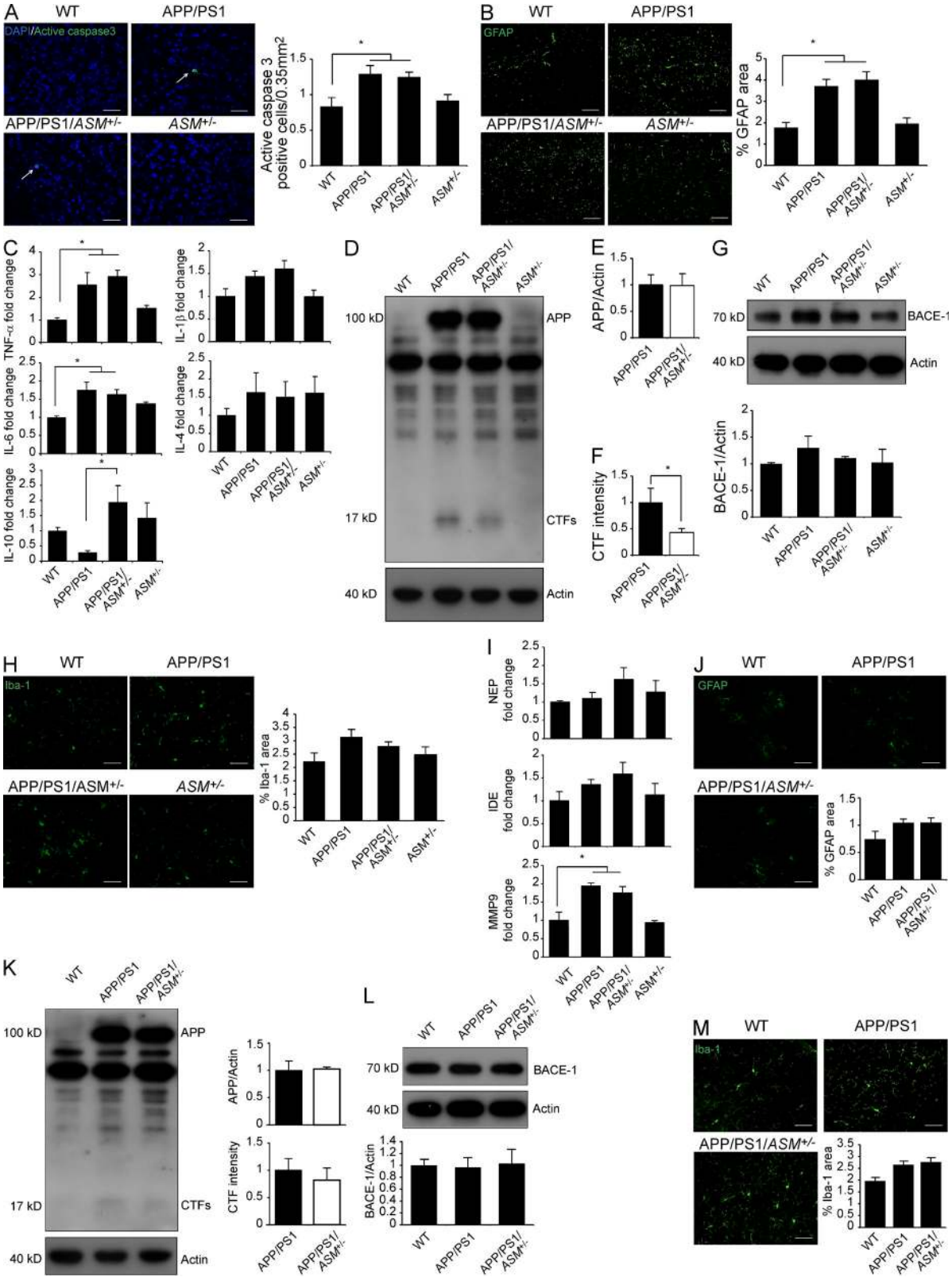

Figure 4. Genetic inhibition of ASM does not affect inflammatory pathway and processing of APP. Brain sections of APP/PS1 and APP/PS1/*ASM*$^{+/-}$ mice were stained with active caspase3 (A; $n = 5$ per group; bars, 50 µm; arrows indicate active caspase3-positive cells) and GFAP antibody (B; $n = 6$ per group; bars, 100 µm). (C) mRNA levels of proinflammatory cytokines or antiinflammatory cytokines ($n = 4$–5 per group). (D) Mouse brain lysates were tested for APP and β-CTF levels using Western blot analysis. (E and F) Quantification of APP (E) and β-CTF (F) levels ($n = 6$ per group). (G) Western blot analysis for Bace-1 levels ($n = 6$ per

the two strains (Fig. 4, A–C). To determine whether reduction of ASM activity affected APP expression, we compared the levels of APP in the two strains. We found that partial genetic inhibition of ASM did not influence the overall expression levels of APP (Fig. 4, D and E). We also examined the Aβ generating enzyme Bace-1 using brain homogenates. Bace-1 was slightly decreased in APP/PS1/*ASM*$^{+/-}$ mice compared with APP/PS1 mice, but the reduction did not reach statistical significance (Fig. 4 G). To address Aβ clearance by microglia, we analyzed microglia activation and Aβ degrading enzyme release by microglia but again did not detect differences (Fig. 4, H and I). Similarly, these changes did not show any differences between APP/PS1 and APP/PS1/*ASM*$^{+/-}$ mice in 5-mo-old young mice (Fig. 4, J–M). There were also no significant differences of brain pathology, such as apoptosis, inflammation, and Aβ deposition, between the WT and *ASM*$^{+/-}$ mice (Fig. 4, A–I). Overall, these data suggested that the partial inhibition of ASM in APP/PS1/*ASM*$^{+/-}$ did not alter major inflammatory pathways or expression of APP.

Dysfunction of the normal proteolytic degradation system also could affect AD pathogenesis and lead to enhanced Aβ deposition (Lee et al., 2010b). Autophagy, a major degradative pathway of the lysosomal system, is known to be markedly impaired in AD (Boland et al., 2008). We found that the microtubule-associated protein 1 light chain 3 (LC3)–II levels were significantly increased in human AD-derived fibroblasts compared with control fibroblasts (Fig. 5, A–C). Increased LC3-II levels could stem from overinduction of autophagy or may be a product of reduced autophagic turnover and defects in the latter stages of autophagic degradation. We therefore measured the level of beclin-1 expression in the AD cells, which is part of a kinase complex responsible for autophagy induction (Zeng et al., 2006), and found that it did not vary between the groups (Fig. 5, A and B).

To examine autophagic turnover of protein, we then analyzed proteolysis of long-lived proteins (Lee et al., 2010b) in control and AD fibroblasts. When autophagic/lysosomal degradation was induced through serum withdrawal, proteolysis was increased in control fibroblasts but not significantly changed in PS1 and apolipoprotein E4 (ApoE4)–derived AD patient fibroblasts (Fig. 5 D). Lysosome stability relating to autophagy also could be affected by lysobisphosphatidic acid (LBPA) binding with ASM (Kirkegaard et al., 2010). We therefore measured LBPA immunofluorescence intensity in control and AD fibroblasts, and found that it did not vary between the groups (Fig. 5 E). Collectively, these data indicated that the autophagosome accumulation in AD is due to dysregulation of autophagic protein degradation, similar to previous results (Lee et al., 2010b).

To examine how genetic inhibition of ASM affected the autophagic pathway in AD, we also analyzed fibroblasts and brain samples derived from 9-mo-old WT, APP/PS1, APP/PS1/*ASM*$^{+/-}$, and *ASM*$^{+/-}$ mice. Compared with WT, APP/PS1 mice showed increased LC3-II, similar to human AD fibroblasts. This enhanced LC3-II level was reduced in APP/PS1/*ASM*$^{+/-}$ mice. Beclin-1 expression did not vary between the groups (Fig. 5, F, G, K, and L). Metabolic analysis of protein turnover (Cuervo et al., 2004) was assessed using fibroblasts from WT, APP/PS1, and APP/PS1/*ASM*$^{+/-}$ mice. Under culture conditions that induced autophagy (absence of serum), degradation of long-lived proteins was significantly lower in cells from APP/PS1 mice compared with WT mice but was increased in cells derived from APP/PS1/*ASM*$^{+/-}$ mice (Fig. 5 I). The differences of cell senescence levels in cultured mice fibroblasts were not found between the groups, indicating that these changes were not related to the cell senescence (Fig. 5 J). The levels of cathepsin D, a lysosomal hydrolase, were elevated in APP/PS1 mice compared with WT. Enhanced cathepsin D level was ameliorated in APP/PS1/*ASM*$^{+/-}$ mice (Fig. 5, F, G, K and L). However, the activity of cathepsin D was not changed between the groups (Fig. 5, H and M). This result indicates that the elevated levels of cathepsin D in APP/PS1 mice did not ultimately translate into a significant increase of enzyme activity. We also analyzed the expression of p62, indicator of autophagic turnover. Increased p62 levels in APP/PS1 mice were reduced in APP/PS1/*ASM*$^{+/-}$ mice (Fig. 5, F, G, K and L).

To corroborate the immunoblotting results, we performed electron microscope (EM) analysis using mouse brain samples. As previously reported (Yu et al., 2005), APP/PS1 mouse brain regions showed an increased number of autophagic vacuoles (AVs), whereas brains of APP/PS1/*ASM*$^{+/-}$ mice showed a reduced number of these vesicles, albeit still higher than WT mice (Fig. 5 N).

The endocytic pathway is also considered a major contributor to Aβ deposition in AD (Ginsberg et al., 2010; Li et al., 2012). To determine whether the endocytic pathway was affected by partial ASM inhibition, we examined Rab5 and Rab7 expression in our animals. The expression pattern of these proteins showed no difference between the groups (Fig. 5 O). Although additional studies of endocytic pathway are required to identify the exact mechanism, our results showed that endocytic pathway was not a main mechanism by ASM inhibition. Collectively, these results revealed dysfunctional changes in the turnover of AVs in the APP/PS1 mice, and that partial genetic ASM inhibition could reverse this abnormality and improve autophagic degradation of proteins.

group). (H) Immunofluorescence images of Iba-1 in the APP/PS1 and APP/PS1/*ASM*$^{+/-}$ mouse brain (bars, 100 µm). The relative area occupied by Iba-1–positive cells was quantified (n = 6 per group). (I) The expression of NEP, IDE, and MMP9 was measured in the brain with quantitative real-time RT-PCR (n = 4–5 per group). (J) Immunofluorescence images of GFAP-positive cells in the 5-mo-old WT, APP/PS1, and APP/PS1/*ASM*$^{+/-}$ mouse brain (bars, 100 µm). The relative area occupied by GFAP-positive cells was quantified (n = 6–7 per group). (K) Western blot analysis and quantification for APP and β-CTF levels in the 5-mo-old mice (n = 6 per group). (L) Western blot analysis for Bace-1 levels in the 5-mo-old mice (n = 6 per group). (M) Immunofluorescence images of Iba-1 in the in the 5-mo-old mouse brain (bars, 100 µm). The relative area occupied by Iba-1–positive cells was quantified (n = 6 per group). Data are representative of three (A–H) or two (J–M) independent experiments. A–C, G–J, L, and M, one-way ANOVA, Tukey's post hoc test. E, F, and K, Student's t test. *, $P < 0.05$. All error bars indicate SEM.

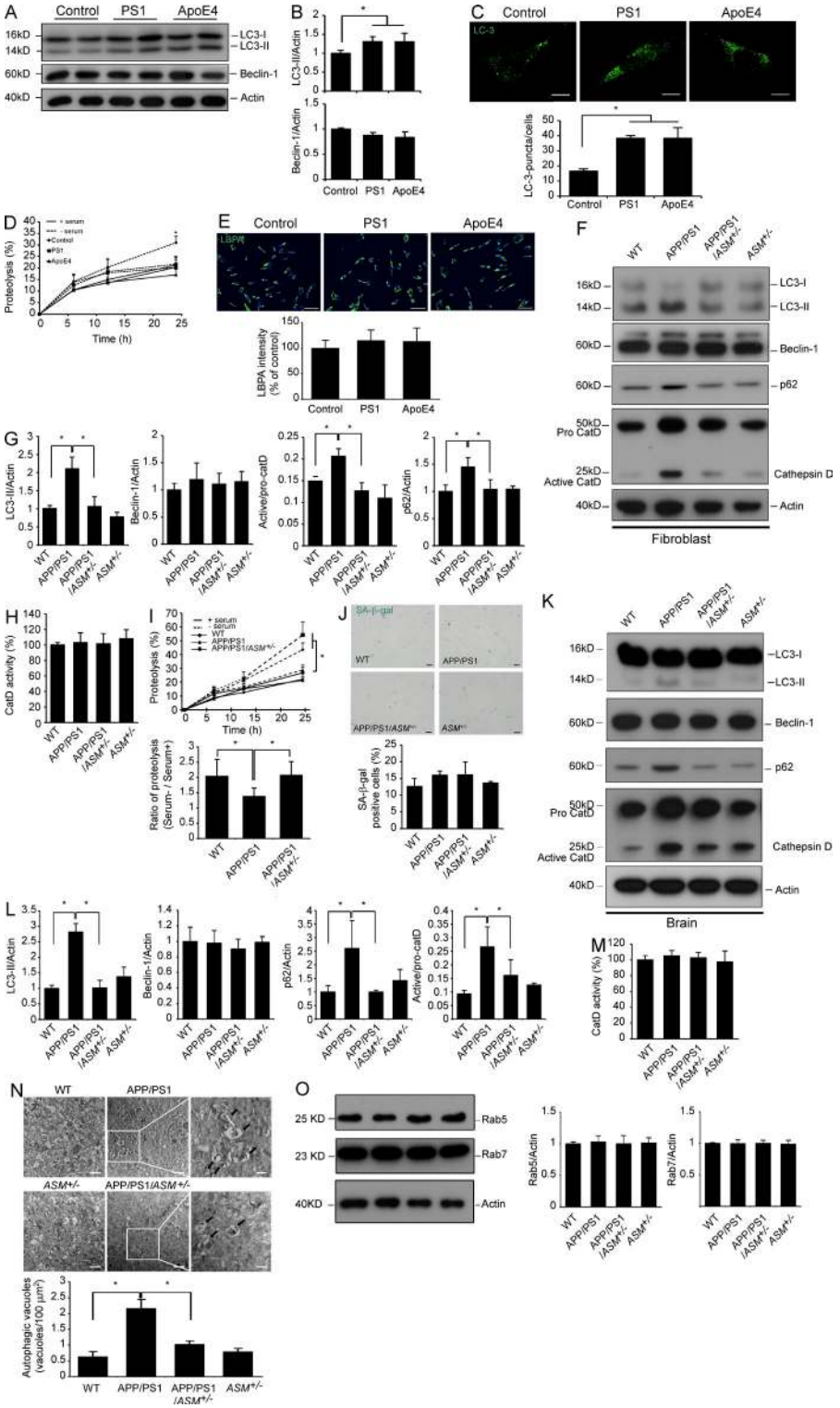

Figure 5. Partial genetic inhibition of ASM reverses defective autophagy in APP/PS1 mice. (A) Western blot analysis of LC-3 and beclin-1 levels in controls, PS1-FAD, and ApoE4 fibroblasts. (B) LC3-II and beclin-1 levels were quantified (n = 4 per group). (C) Immunocytochemistry for LC3 in controls, PS1-FAD, and ApoE4 fibroblast (n = 4–5 per group; bars, 20 μm). (D) Degradation of long-lived proteins was measured in controls, PS1-FAD, and ApoE4 fibroblasts (n = 6 per group). (E) Representative images and quantification of LBPA in control, PS1-FAD, and ApoE4 fibroblast (n = 4 per group; bars, 50 μm). (F) Western blot analyses for LC3, beclin-1, p62, and cathepsin D in tail fibroblast derived from WT, APP/PS1, *ASM*$^{+/-}$, and APP/PS1/*ASM*$^{+/-}$ mice. (G) Densitometric analysis of LC-3-II, beclin-1, p62, and cathepsin D (n = 7–8 per group). (H) Cathepsin D activity in mice tail fibroblast (n = 4 per group). (I) Rates of proteolysis of long-lived proteins in fibroblasts (n = 6 per group). (J) Representative images and quantification data of SA-β-gal staining in the mice tail fibroblasts (n = 5 per group; bars, 50 μm). (K) Western blot analyses for LC3, beclin-1, p62, and cathepsin D in the brains of 9-mo-old WT, APP/PS1, *ASM*$^{+/-}$, and APP/PS1/*ASM*$^{+/-}$ mice. (L) Densitometric quantification of LC-3-II, beclin-1, p62, and cathepsin D (n = 6–8 per group). (M) Cathepsin D activity in brain extracts of WT, APP/PS1, *ASM*$^{+/-}$, and APP/PS1/*ASM*$^{+/-}$ mice (n = 4 per group). (N) EM images and quantification data of cortical region. Higher magnification of boxed area shows detail of AVs (arrow; n = 5 per group; bars: [low magnification] 2 μm, [high magnification] 1 μm). (O) Western blot analysis of Rab5 and Rab7 levels in the brain lysates (n = 5 per group). Data are representative of two (A–E and N) or three (F–M and O) independent experiments. B–O, one-way ANOVA, Tukey's post hoc test. *, $P < 0.05$. All error bars indicate SEM.

ASM elevation causes defective autophagic degradation by lysosomal depletion

To gain more direct insights into the relationship of ASM and autophagic dysfunction, we treated human fibroblasts and neurons with recombinant 1–10 μM ASM and determined the LC3-II and p62 levels. ASM strongly accelerated LC3-II and p62 levels in human fibroblasts and neurons in a concentration-dependent manner (Fig. 6, A–C). The level of beclin-1 expression was not affected by ASM (Fig. 6, A and C), indicating that the accumulation of autophagosomes was not due to the biogenesis pathway. ASM is found in a secretory and a lysosomal form (Jenkins et al., 2009), and the mannose-6-phosphate (M6P)

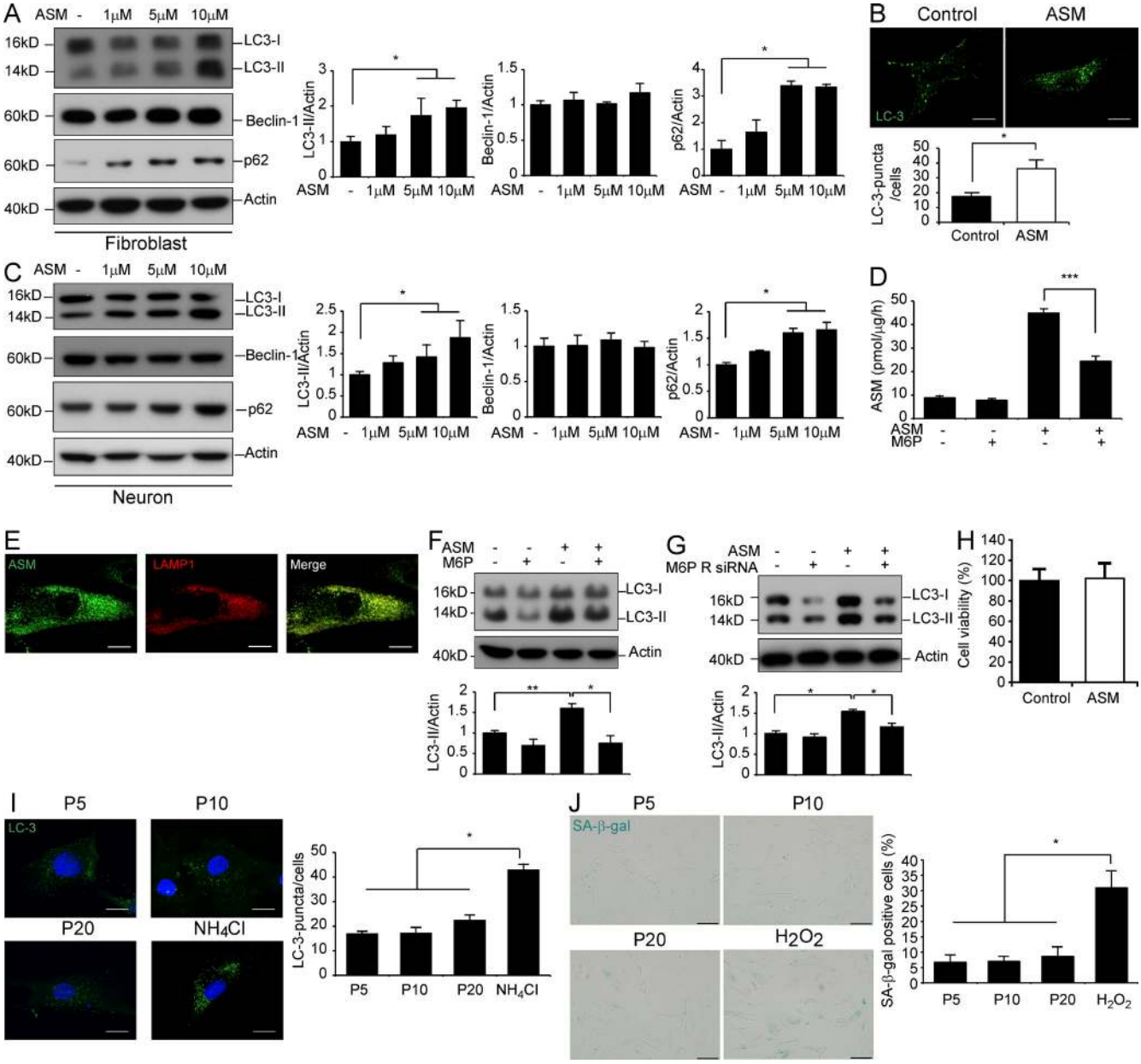

Figure 6. Autophagic processes are affected by lysosomal ASM. (A and C) Western blot analysis of LC3, Beclin-1, and p62 in human fibroblast (A; *n* = 7 per group) and human neuron (C; *n* = 6 per group). (B) Immunocytochemistry and quantification for LC3 after ASM treatment (*n* = 7–8 per group; bars, 20 µm). (D) ASM activity was assessed in the ASM-treated fibroblast with or without M6P (*n* = 6 per group). (E) Confocal microscopic analysis of Lamp1- and ASM-positive vesicles (bars, 20 µm). (F and G) The effect of lysosomal ASM on LC3-II expression. (F) 10 µM ASM was added to fibroblast for 24 h with or without 10 mM M6P. LC3-II expression was determined by Western blot analysis (*n* = 5–6 per group). (G) LC3-II levels were examined in 10 µM ASM-treated fibroblast with or without M6P receptor suppression using siRNA (*n* = 5–6 per group). (H) The effect of 10 µM ASM on cell viability was estimated by MTT assay (*n* = 5–6 per group). (I and J) Representative images and quantification data of LC3 (I; bars, 20 µm) and SA-β-gal staining (J; bars, 100 µm) in P5, P10, and P20 human fibroblasts. NH_4Cl and H_2O_2 were used for positive control (*n* = 5 per group). Data are representative of three (B, E, I, and J) or four (A, C, D, and F–H) independent experiments. A, C, F, G, I, and J, one-way ANOVA, Tukey's post hoc test. B, D, and H, Student's *t* test. *, $P < 0.05$; **, $P < 0.01$; ***, $P < 0.005$. All error bars indicate SEM.

receptor system is involved in trafficking of ASM to the lysosome (Dhami and Schuchman, 2004). To elucidate which ASM form affected lysosomal/autophagic dysfunction, cells were incubated with ASM alone, or in the presence of M6P. As expected, the activity of ASM was significantly increased in ASM-treated cells compared with nontreated cells. This enhanced ASM activity was reduced in the presence of M6P (Fig. 6 D). To confirm whether the ASM treatment reached the lysosomes, we also examined the colocalization of ASM and lysosomes using immunocytochemistry. Double immunostaining

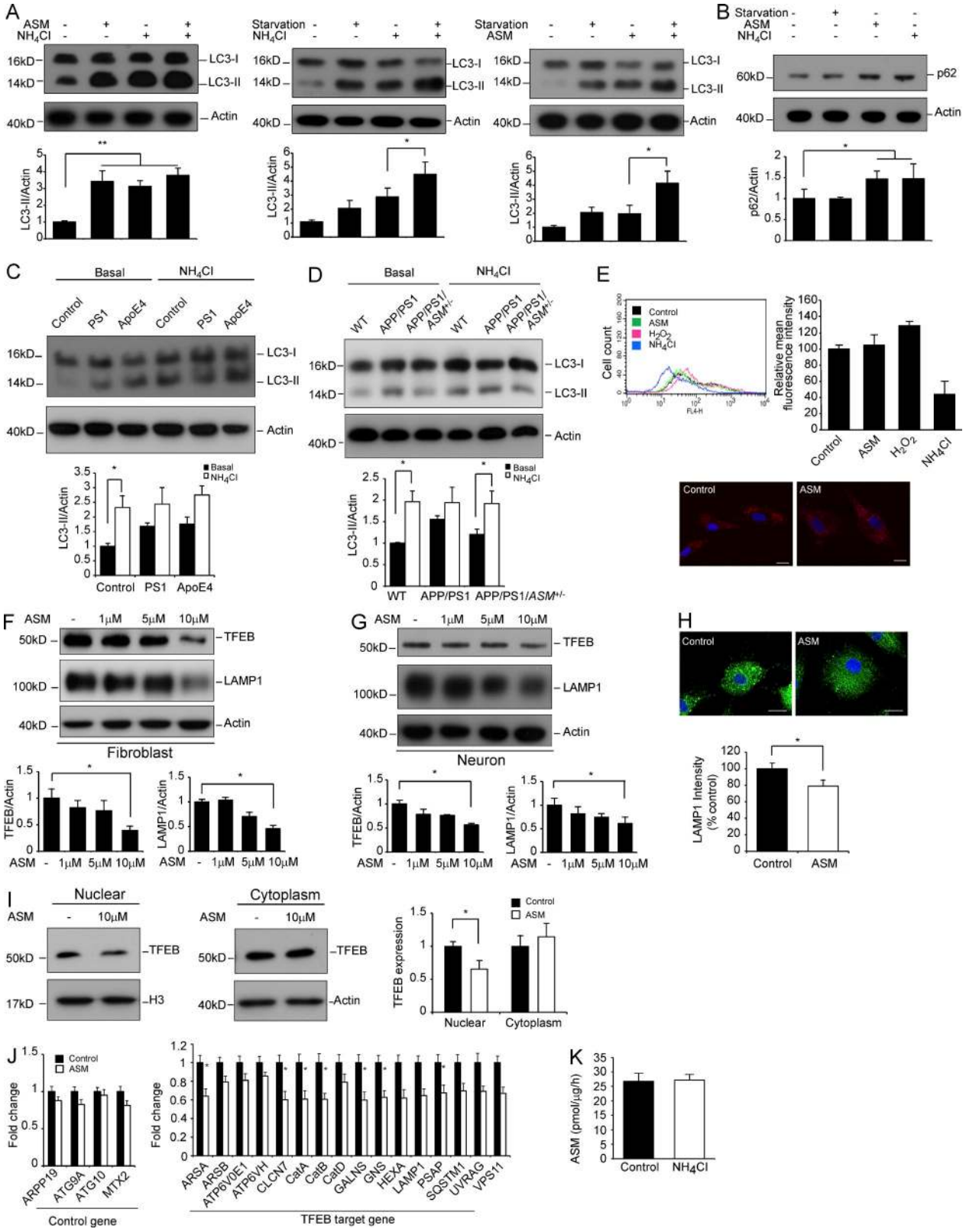

Figure 7. ASM causes abnormal autophagic protein degradation by altering ALP. (A) Autophagic flux assay. Human fibroblasts were cultured in: (1) complete medium with or without 10 μM ASM in the presence or absence of NH_4Cl (left), (2) complete medium or starvation condition in the presence or absence of NH_4Cl (middle), or (3) complete medium or starvation condition with or without 10 μM ASM (right). The LC3-II levels were examined by Western blotting (n = 6–7 per group). (B) The accumulation of p62 was assessed in the human fibroblast cultured with 10 μM ASM, 20 mM NH_4Cl, or starvation

of ASM and lysosomal-associated membrane protein 1 (Lamp1) showed that most ASM-positive vesicles were colocalized with Lamp1-positive vesicles, indicating that treated ASM was located in lysosome (Fig. 6 E). The ASM-induced autophagosome accumulation was significantly decreased by inhibition of lysosomal ASM uptake using M6P or M6P receptor siRNA (Fig. 6, F and G). These results suggested that elevation of lysosomal ASM may lead to autophagic dysfunction in AD. ASM treatment did not affect the cell survival (Fig. 6 H). The levels of LC3 and cell senescence in the fibroblast also did not show the differences with passage number, indicating that ASM caused the abnormal autophagy (Fig. 6, I and J).

As discussed above, the accumulation of AVs in cells can result from either autophagy induction or the blockade of autophagic degradation. To further distinguish between these possibilities, we performed an autophagic flux assay (Rubinsztein et al., 2009) in the presence or absence of NH_4Cl that blocks autophagic degradation but does not affect autophagosome formation. It was hypothesized that if ASM treatment enhanced autophagy induction, in the presence of NH_4Cl (which inhibits degradation) a considerable increase in LC3-II would be expected due to the combined effects of blocking degradation and enhancing induction. However, compared with NH_4Cl treatment alone, dual treatment of fibroblasts with ASM and NH_4Cl did not show any significant changes of LC3-II (Fig. 7 A, left). In contrast, the addition of NH_4Cl (Fig. 7 A, middle) or ASM (Fig. 7 A, right) in serum starvation culture resulted in a significant but similar increase of LC3-II levels. Furthermore, we measured the autophagic flux by detecting the abundance of p62. The levels of p62 were markedly increased in the cells treated with ASM or NH_4Cl (Fig. 7 B). We also performed LC3 flux assay in human AD fibroblasts and 9-mo-old WT, APP/PS1, and APP/PS1/$ASM^{+/-}$ mice fibroblasts. Autophagic flux was measured by assessing the changes of LC3-II in the presence and absence of NH_4Cl–mediated lysosomal inhibition. Under basal condition, human AD and APP/PS1 fibroblasts showed significantly increased LC3-II levels compared with normal cells. NH_4Cl–induced lysosome inhibition led to marked increase of LC3-II levels in the normal fibroblasts, but this increase was significantly less in the AD cells (Fig. 7, C and D). APP/PS1/$ASM^{+/-}$ fibroblast showed similar pattern in LC3-II increase compared with normal cell (Fig. 7 D). Collectively, these results indicated that enhanced lysosomal ASM in AD caused a defect of autophagic degradation but not induction.

To further investigate the relationship of elevated ASM and defective lysosomal/autophagic degradation, we evaluated alteration in lysosomal pH using the acidotropic dye LysoTracker red. H_2O_2- and NH_4Cl-treated cells were used as positive and negative controls, respectively. Flow cytometry and fluorescent microscopic analysis did not show any differences of lysosomal pH between ASM- and vehicle-treated fibroblast (Fig. 7 E). Recently, the transcription factor EB (TFEB) was identified as a master regulator of the autophagy–lysosome pathway (ALP) and lysosome biogenesis (Settembre et al., 2011). Enhancement of TFEB function is able to stimulate ALP function and promote protein clearance. To examine whether ASM could affect the ALP and lysosome biogenesis, we tested endogenous levels of TFEB. ASM-treated fibroblasts and neurons showed significantly decreased TFEB levels (Fig. 7, F and G). Also, the levels of the lysosomal structural protein Lamp1 were decreased in ASM-treated cells (Fig. 7, F–H). To further validate our observation, we investigated TFEB subcellular localization after ASM treatment. Interestingly, ASM-treated cells showed a reduced TFEB expression in the nuclear compartment (Fig. 7 I). Similarly, the expression levels of TFEB target genes related to lysosome were significantly decreased in ASM-treated fibroblasts (Fig. 7 J). Conversely, to determine whether autophagic degradation affected ASM, we evaluated ASM activity in fibroblasts after NH_4Cl treatment. Blocking of autophagic degradation via NH_4Cl did not show any significant changes of ASM activity (Fig. 7 K). These results further suggested that lysosomal ASM acts not as an inducer but rather as an inhibitor of autophagic protein degradation by reducing ALP function and lysosome biogenesis.

To examine the in vivo effect of ASM activation on autophagic dysfunction, we introduced conditioned medium (CM) from cultured ASM-overexpressing cells into C57BL/6 mice via intracerebral (i.c.) and intravenous (i.v.) injections. ASM-CM–treated mice showed elevated ASM activity in the brain and plasma (Fig. 8, A and B), as well as increased LC3-II without changes of beclin-1 expression in the brains (Fig. 8, C and D). Cathepsin D level was increased in the ASM-CM (i.c.)–treated mice compared with control mice, but actual activity was not changed (Fig. 8, C and E). p62 also was increased in the ASM-CM (i.c.)–treated mice compared with control mice (Fig. 8 C). ASM-CM (i.c.)–treated mice further exhibited abnormal ALP function, indicative of decreased TFEB and Lamp1 levels (Fig. 8 F). Although ASM-CM (i.v.)–treated mice showed slightly increased cathepsin D and p62

condition (n = 4 per group). (C) Western blot analysis of LC3-II levels in controls, PS1-FAD, and ApoE4 fibroblasts in the presence or absence of NH_4Cl (n = 6 per group). (D) Western blot analysis for LC3-II levels in fibroblasts derived from WT, APP/PS1, and APP/PS1/$ASM^{+/-}$ mice in the presence or absence of NH_4Cl (n = 6 per group). (E) Effect of ASM on lysosomal pH. FACS and histological analysis of fibroblasts stained with LysoTracker red (n = 5 per group; bars, 20 µm). H_2O_2- and NH_4Cl-treated cells were used as positive and negative controls, respectively. (F and G) Western blot analyses for TFEB and Lamp1 in human fibroblasts (F; n = 6 per group) and neurons (G; n = 6 per group) after treatment with ASM. (H) Immunocytochemistry of Lamp1 in control and ASM-treated fibroblast (n = 5 per group; bars, 20 µm). (I) Western blot analysis for nuclear localization of TFEB in ASM-treated cells (n = 5 per group). (J) Quantitative real-time PCR analysis of TFEB-target gene expression in normal (n = 6) and ASM-treated (n = 10) fibroblasts. (K) ASM activity was estimated in the fibroblast with or without NH4Cl (n = 5 per group). Data are representative of two (E, H, and I) or three (A–D, F, G, J, and K) independent experiments. A, B, and E–G, one-way ANOVA, Tukey's post hoc test. C, D, and H–K, Student's t test. *, $P < 0.05$; **, $P < 0.01$. All error bars indicate SEM.

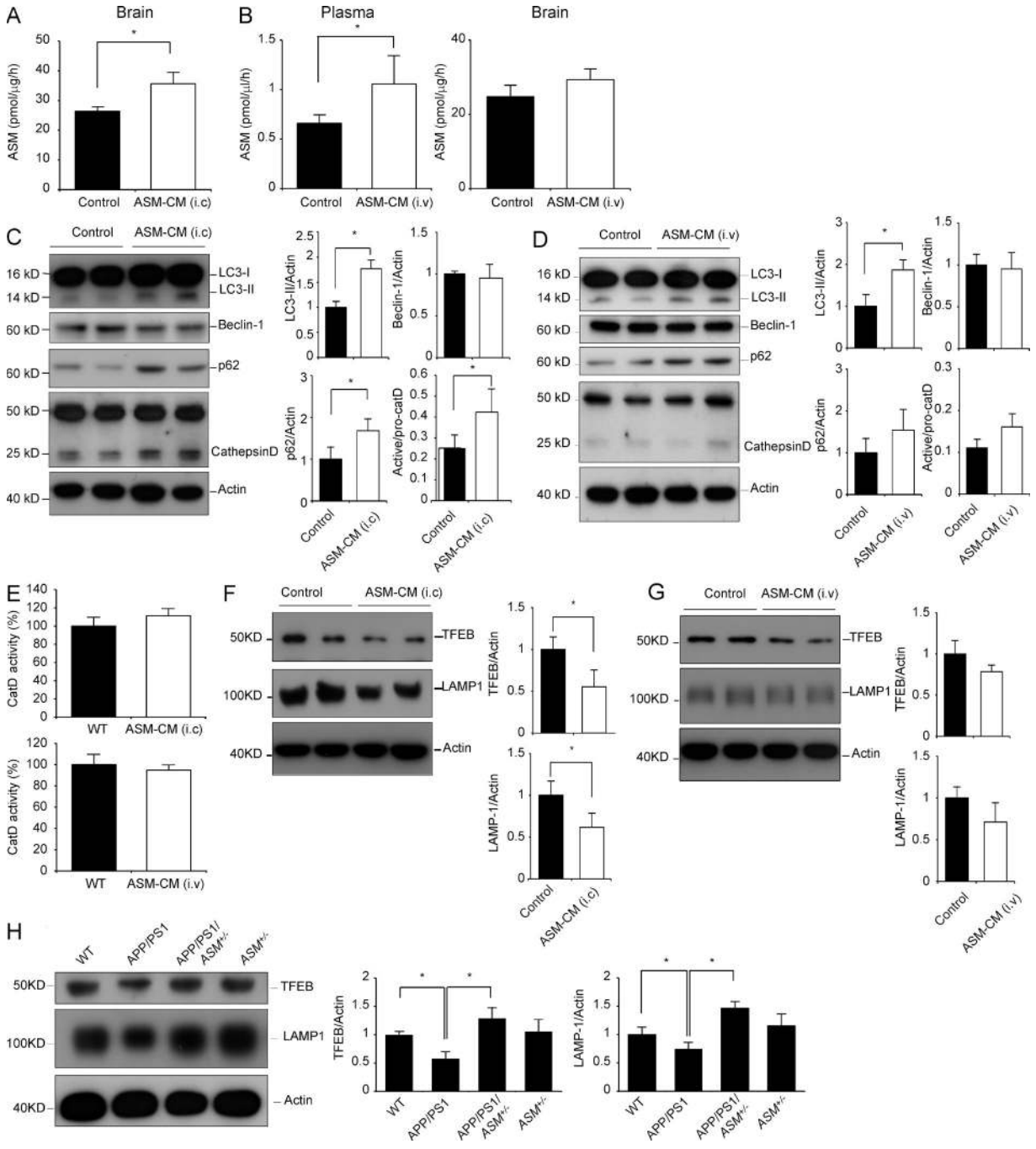

Figure 8. ASM causes autophagic dysfunction in vivo by sequestrating ALP function. (A and B) ASM was estimated in the brain and blood plasma of C57BL/6 mice after ASM-CM treatment into the hippocampus (A; i.c., $n = 6$ per group) or tail vein (B; i.v., $n = 6$ per group). (C and D) Western blot analyses for LC3, beclin-1, p62, and cathepsin D in the brains of C57BL/6 mice after ASM-CM treatment into the hippocampus (C; $n = 5–6$ per group) or tail vein (D; $n = 4–5$ per group). (E) Cathepsin D activity in the brain extracts of C57BL/6 mice after ASM-CM treatment ($n = 4$ per group). (F and G) Protein expression of TFEB and Lamp1 in the brains after ASM-CM treatment into the hippocampus (F; $n = 5–6$ per group) or tail vein (G; $n = 5$ per group). (H) Protein expression of TFEB and Lamp1 in the brains of 9-mo-old WT, APP/PS1, $ASM^{+/-}$, and APP/PS1/$ASM^{+/-}$ mice ($n = 6–7$ per group). Data are representative of three independent experiments. A–G, Student's *t* test. H, one-way ANOVA, Tukey's post hoc test. *, $P < 0.05$. All error bars indicate SEM.

levels and decreased ALP function proteins, this did not reach statistical significance (Fig. 8, D and G). The activity of cathepsin D was also not changed (Fig. 8 E). These relatively modest effects of ASM-CM (i.v.) treatment on autophagy dysfunction might be due to presence of the blood–brain barrier because only a slight increase of ASM activity in the brain was achieved by these treatments, and the activity of ASM did not reach those of APP/PS1 mice.

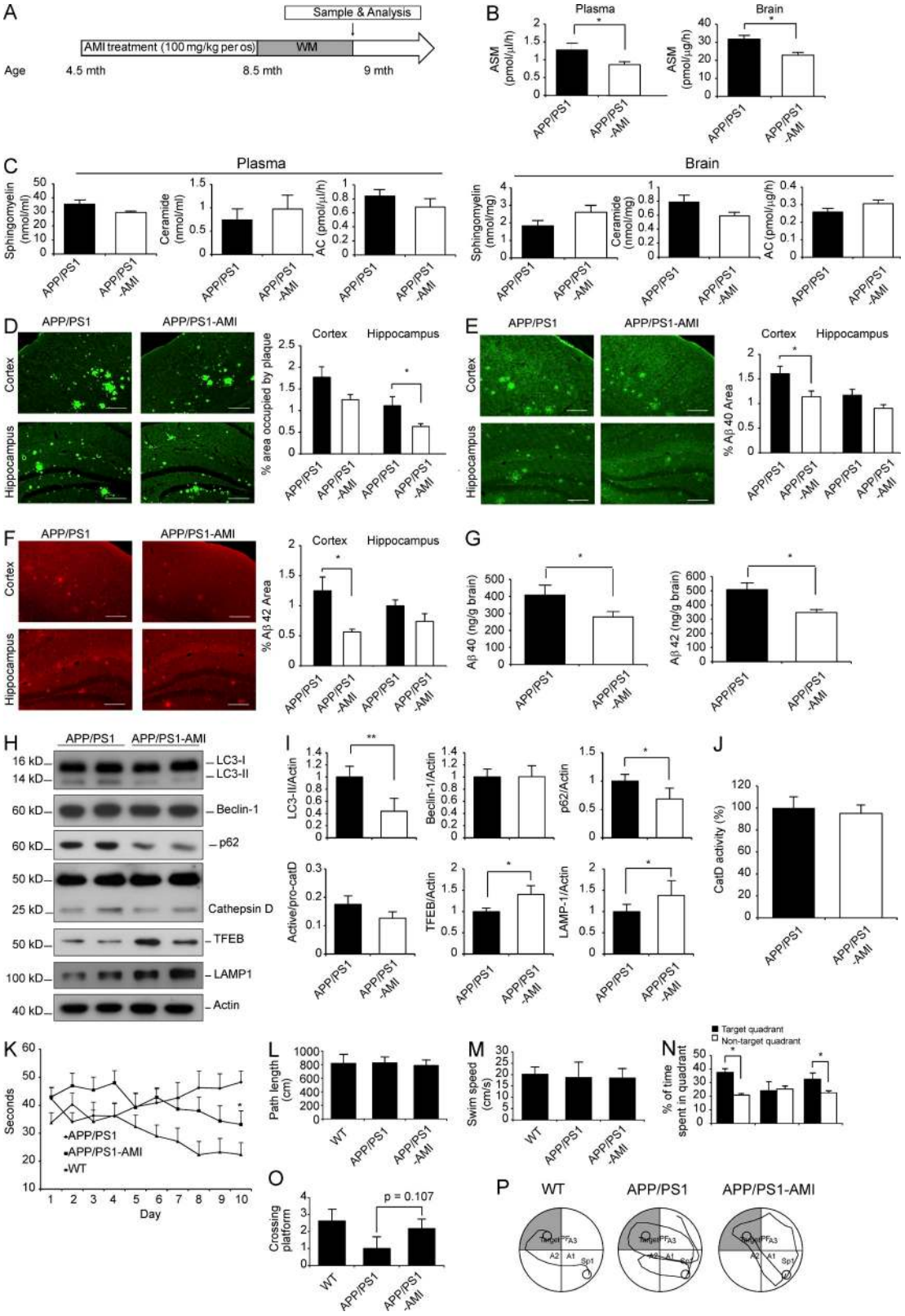

Figure 9. Pharmacological restoration of ASM to the normal range improves pathology in AD mice. (A) Protocol of AMI treatment in APP/PS1 mice. (B) ASM was estimated in the blood plasma (n = 12–14 per group) and brain (n = 9–10 per group) of APP/PS1 mice after AMI treatment. (C) Sphingomyelin, ceramide, and AC were determined using UPLC based methods in the plasma (n = 9 per group) and brain (n = 8 per group). (D) Mice brain sections were stained with thioflavin S to detect Aβ (bars, 200 μm). The relative area occupied by Aβ plaques were determined (n = 6 per group). (E–G) Aβ40

To examine whether partial genetic inhibition of ASM affected the ALP in APP/PS1 mice, we also analyzed TFEB and Lamp1 levels in the brain samples derived from WT, APP/PS1, $ASM^{+/-}$, and APP/PS1/$ASM^{+/-}$ mice. Compared with WT, APP/PS1 mice showed significantly decreased TFEB and Lamp1 expression, which were increased in APP/PS1/$ASM^{+/-}$ mice (Fig. 8 H). Together, these findings show for the first time a direct correlation of lysosomal ASM and the function of the ALP, and suggest that abnormal autophagic degradation in AD may be due to the effects of elevated ASM expression on this pathway.

Pharmacological restoration of ASM to the normal range improves pathology in AD mice

The ASM-mediated lysosomal/autophagic dysfunction in AD prompted us to examine possible therapeutic implications of this pathway. To decrease ASM in APP/PS1 mice, we undertook pharmacological inhibition using amitriptyline-hydrochloride (AMI) for 4 mo (Fig. 9 A). AMI is a known inhibitor of ASM that can cross the blood–brain barrier. At 9 mo of age, AMI-treated APP/PS1 mice exhibited decreased ASM activity compared with vehicle-treated mice (Fig. 9 B). Other sphingolipid metabolites were not changed (Fig. 9 C). Aβ levels were decreased in the AMI-treated APP/PS1 mice compared with the nontreated littermates (Fig. 9, D–G). The levels of LC3-II, p62, and cathepsin D were decreased in the AMI-treated APP/PS1 mice (Fig. 9, H and I). Actual activity of cathepsin D was not changed by AMI treatment (Fig. 9 J). AMI treatment significantly increased TFEB and Lamp1 protein levels in APP/PS1 mice (Fig. 9, H and I). Similarly, APP/PS1 mice treated with AMI showed recovery of memory function (Fig. 9, K–P). Overall, these positive but relatively moderate results (e.g., Aβ levels) in AMI-treated APP/PS1 mice might be due to under dosing of the animals. We speculate that this may be improved in the future by adjusting the dose or using modified, more potent drugs of a similar class.

Restoration of ASM ameliorates autophagic dysfunction in the AD patient–specific cells

To further validate our observation made by partial ASM inhibition in AD mice, we studied possible changes in autophagy dysfunction in human AD fibroblast after ASM inhibition. Elevated ASM levels in human AD fibroblasts (PS1–familial AD [FAD] and ApoE4) were restored to normal range by ASM siRNA treatment (Fig. 10 A). ASM siRNA-treated human AD fibroblasts (PS1-FAD and ApoE4) showed decreased LC3-II and p62 accumulation compared with control siRNA-treated cells (Fig. 10 B). Also, ASM siRNA was able to increase lysosome levels (as judged by Lamp1 expression) by activating TFEB in the human AD fibroblasts (Fig. 10 C).

Many insights into the pathogenesis in neurodegenerative disease have come from investigating postmortem brain tissues due to the difficulty of invasive access to living human CNS. The recent developments in induced pluripotent stem cells (iPSCs) and induced neurons have allowed investigation of pathogenesis of neurological diseases in vitro (Kondo et al., 2013). To explore whether the observed effects of ASM in previous results are paralleled by similar alterations in AD human neurons, we first established iPSCs with PS1 mutation (PS1 iPSC-2, -4, and -21) by transduction of human fibroblast with retroviruses encoding OCT4, SOX2, KLF4, and c-Myc. The PS1-iPSC cell line was shown to be fully reprogrammed to pluripotency, as judged by colony morphology, alkaline phosphatase (AP) staining, expression of pluripotency-associated transcription factors and surface markers, karyotype stability, and generation of teratomas (Fig. 10, D–G). To establish whether the PS1 mutation may affect neuronal differentiation, PS1 iPSC and control iPSC lines were induced to differentiate into neurons for 10 d. Consistent with previous results (Kondo et al., 2013), no obvious differences in the ability to generate neurons were observed between control and PS1-iPSCs (Fig. 10 H). Aβ42 secretion level was increased in PS1 iPSC-derived neurons compared with control iPSC-derived neuron (Fig. 10 I).

Next, we investigated whether elevated ASM in fibroblasts was also evident increased in PS1 iPSC and iPSC-derived neurons. The ASM activity in PS1 iPSC was not changed except for PS1-4 iPSC in comparison to those in control iPSC, but the activity of ASM was significantly higher in PS1 iPSC-derived neurons compared with control iPSC-derived neuron (Fig. 10 J). Elevated ASM levels in PS1 iPSC-derived neurons were restored to normal range by ASM siRNA treatment (Fig. 10 J). Neurons from PS1-4 iPSCs also had significantly higher abnormal autophagic markers than neurons from control iPSC (Fig. 10 K). ASM siRNA treatment significantly decreased the protein level of abnormal autophagic markers in PS1 iPSC-derived neurons (Fig. 10 K). To corroborate the immunoblotting results, we performed EM analysis using control and PS1 iPSC-derived neurons. As expected, PS1 iPSC-derived neurons exhibited increased AV accumulation, whereas ASM siRNA-treated PS1 iPSC-derived neurons showed a reduced number of these vesicles (Fig. 10 L).

and Aβ42 in the brains of AMI treated or nontreated APP/PS1 mice were assessed using immunofluorescence staining (E and F; $n = 8$ per group; bars, 200 µm) and ELISA kits (G; $n = 6$ per group). (H and I) Western blot analyses and quantification for LC3, Beclin-1, p62, cathepsin D, TFEB, and Lamp1 in the brains of APP/PS1 mice treated with AMI or control ($n = 6$–8 per group). (J) Cathepsin D activity in the brain extracts of AMI-treated or nontreated APP/PS1 mice ($n = 4$ per group). (K) Escape latencies of APP/PS1 mice treated with AMI or control over 10 d (WT, $n = 14$; nontreated APP/PS1, $n = 10$; and AMI-treated APP/PS1, $n = 12$). (L–O) Probe trial day 11. (L and M) Path length (L) and swim speed (M) were recorded and analyzed. (N) Time spent in target platform and other quadrants was measured. (O) The number of times each animal entered the small target zone during the 60-s probe trial. (P) Representative swimming paths at day 10 of training. Data are representative three independent experiments. B–J and N, Student's *t* test; K–M and O, one-way ANOVA, Tukey's post hoc test. *, $P < 0.05$; **, $P < 0.01$. All error bars indicate SEM.

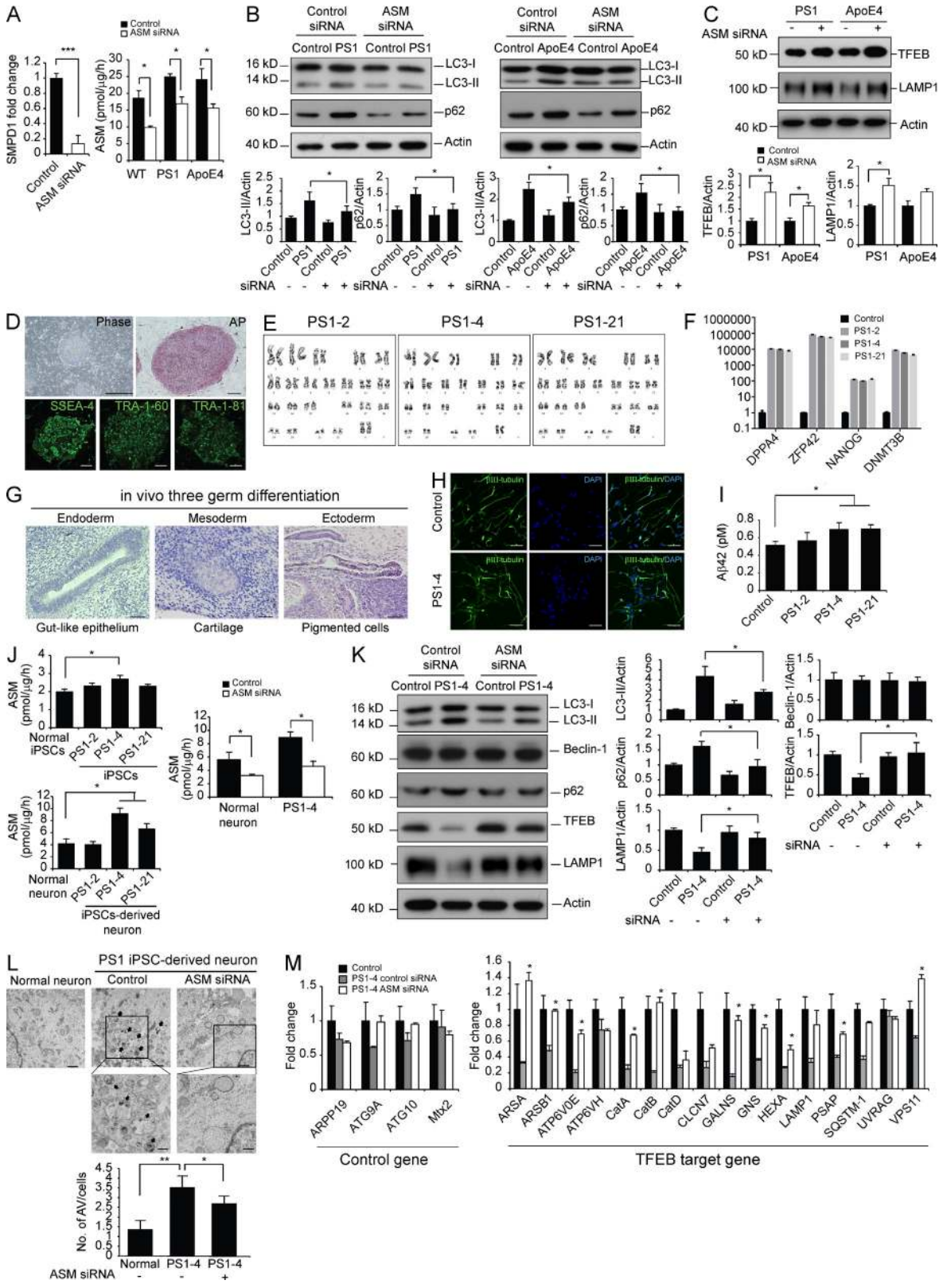

Figure 10. Restoration of ASM to the normal level reverses impaired autophagy in the AD patient-specific cells. (A) SMPD1 gene suppression by ASM-siRNA in human fibroblasts. ASM activity was assessed after ASM siRNA treatment in the control and AD fibroblast (n = 6 per group). (B) LC3-II and p62 levels were examined in human AD fibroblast with or without ASM inhibition. siRNA-mediated suppression of ASM reduced LC3-II and p62 levels in PS1-FAD (left; n = 7 per group) and ApoE4 fibroblast (right; n = 6 per group). (C) Protein expression of TFEB and Lamp1 in the PS1-FAD and ApoE4

Decreased TFEB target genes in PS1 iPSC-derived neurons were also significantly increased by ASM siRNA treatment (Fig. 10 M). These results confirm that abnormal autophagy observed in AD mice and human fibroblasts by ASM also occur in AD patient neurons, and restoration of ASM back to normal levels is able to ameliorate autophagic dysfunction by restoring lysosomal biogenesis in AD patient cells.

DISCUSSION

Although the exact causes of AD are unknown, the complex interactions of genetic and environmental factors are likely play important roles in the pathogenesis. ASM activity is known to be increased by environmental stress and in various diseases, and is elevated in AD patients (He and Schuchman, 2012). One downstream consequence of increased ASM is elevated ceramide, contributing to cell death, inflammation, and other common disease findings. Although elevated ASM is known to occur in AD, the cellular mechanisms that link ASM and AD have not been fully characterized. The data presented here suggest a previously unknown role of ASM in the down-regulation of lysosomal biogenesis and inhibition of lysosome-dependent autophagic proteolysis. The findings also establish proof of concept for ASM inhibitor therapy in AD.

Our previous study showed that sphingolipid metabolism was severely impaired in the human AD brain, and that ASM activity was positively correlated with the Aβ levels (He et al., 2010). Consistent with our previous study, we found that ASM was significantly increased in fibroblasts, brain, and/or plasma from patients with AD and in AD mice, although other sphingolipid factors were unaltered. There are some differences between the previous and this study. For example, the previous results showed increased ceramide level in AD, but we could not found significant changes of sphingolipid factors including ceramide in AD compared with normal samples. These differences might be related to the fact that once formed, ceramide can rapidly enter several metabolic pathways. It may be used for either the biosynthesis of complex lipids or broken down into sphingosine, which itself is rapidly converted to sphingosine 1 phosphate.

Accumulation of abnormal AVs has been observed in AD (Lee et al., 2010b; Nixon and Yang, 2011), and the autophagy pathway is increasingly regarded as an important contributor to Aβ-mediated pathogenesis in AD (Yu et al., 2005; Nixon, 2007). Moreover, it has been shown that the abnormal autophagic flux in AD may be due to dysfunction at the late autophagy stage associated with the lysosome (Lai and McLaurin, 2012; Zhou et al., 2012). Similar to previous results (Lee et al., 2010b; Lai and McLaurin, 2012), we found that the impaired autophagic flux in AD was associated with reduced autophagic degradation due to decreased ALP function. In addition, we show for the first time that this is directly linked to elevated ASM activity. Suppression of ASM expression or inhibition of its uptake and delivery to lysosomes using M6P reversed abnormal autophagic degradation. These findings indicate that increased lysosomal ASM plays a negative role in AD by causing autophagic dysfunction, suggesting that therapeutic strategies to restoring ASM activity to the normal range may be beneficial for AD pathology.

This was further studied in the AD mice by finding that partial genetic or systemic inhibition of ASM activities in these animals largely reversed autophagic pathology by restoring ALP function, as well as reducing the accumulation of incompletely digested substrates within the autophagic-lysosomal compartments (e.g., LC3-II and p62). Aβ accumulation also was reduced in response to ASM inhibition, as was cathepsin D expression. There are several challenges associated with interpretation of cathepsin D levels in AD. Although some reports have shown that cathepsin D activities were decreased in AD (Lee et al., 2010b), many studies indicate that cathepsin D is elevated in AD and contributes to the pathogenesis, such as Aβ formation (Cataldo et al., 2004; Lai and McLaurin, 2012; Zhou et al., 2012). A recent paper suggested that COP9 signalosome deficiency increased cathepsin D levels but reduced the autophagic degradation. They suggested that these results were associated with a failure of lysosomal assembly of cathepsin D because only a lysosomal cathepsin D could affect autophagic degradation (Su et al., 2011). In this study, we have found that maturation of cathepsin D was increased in AD mice, but the actual enzyme activity was not changed between the groups. This result indicated that the elevated levels of cathepsin D did not ultimately translate into a significant increase of enzyme activity. Based on these papers and our data, a plausible interpretation of increased cathepsin D in our AD mice is that AD microenvironment attempts to increase cathepsin D synthesis, but this does not have a direct impact on lysosomal function because the activity of the enzyme is unchanged. Therefore,

fibroblast after ASM inhibition (n = 5–6 per group). (D–G) Generation of PS1 iPSC lines from patient fibroblast. (D) Established iPSCs showed embryonic stem cell–like morphology (Phase; bar, 1 mm), AP activity (bar, 200 µm), and expressed pluripotent stem cell markers SSEA4 (bar 100 µm), TRA1-60 (bar 100 µm), and TRA1-81 (bar 100 µm). (E) Normal karyotype of PS1 iPSC. (F) Quantitative real-time PCR analysis of hESC marker gene of PS1 iPSC (n = 3 per group). (G) Gross morphology and hematoxylin-eosin staining of representative teratomas generated from PS1-4 iPSCs (bars, 50 µm). (H) Estimation of neural differentiation from control and PS1-4 iPSCs. Representative images of immunocytochemical staining the β-III tubulin after neural differentiation (bars, 50 µm). (I) The amount of Aβ42 secreted from control iPSC-derived neuron and PS1 iPSC-derived neuron (n = 5 per group). (J) Characterization of ASM activity in the control and PS1 iPSC and iPSC-derived neurons (n = 6 per group). (K) Western blot analyses for LC3, beclin-1, p62, TFEB, and Lamp1 in the control and PS1-4 iPSC–derived neuron after ASM siRNA treatment (n = 5–6 per group). (L) EM images and quantification data of control and PS1 iPSC-derived neurons. Higher magnification of boxed area shows detail of AVs (arrow; n = 4 per group; bars: [low magnification] 1 µm, [high magnification] 500 nm). (M) Quantitative real-time PCR analysis of TFEB-target gene expression in iPSC-derived neurons after ASM siRNA treatment (n = 5–6 per group). Data are representative of two (A, D–G, I, and L), or three (B, C, H, J, K, and M) independent experiments. A, C, F, I, J, and M, Student's t test. B, K, and L, one-way ANOVA, Tukey's post hoc test. *, $P < 0.05$; **, $P < 0.01$; ***, $P < 0.001$. A–K, error bars indicate SEM. L and M, Error bars indicate SD.

enhanced cathepsin D level in our AD mice induced by increased ASM is more likely a compensatory response to an impaired lysosome system. The present study also provides the first evidence of increased ASM activity and autophagic dysfunction in living human (iPSC-derived) neurons derived from AD patients and that restoring normal levels of ASM in AD neurons effectively blocks abnormal autophagy.

Overall, the data presented here show that increased ASM activity in AD contributes to the abnormal lysosomal/autophagic process by leading to dysfunction of ALP. This results in an inability to break down appropriate substrates during the autophagy process. Restoration of ASM effectively blocks AD progression by increasing autophagic degradation. Although the involvement of other ASM-related mechanisms in AD remains to be explored, the data in this study demonstrate that inhibition of ASM improves Aβ clearance and rescues impaired memory in a validated mouse model of AD, suggesting this as a potential therapy for AD patients in the future.

MATERIALS AND METHODS

Mice. Transgenic mouse lines overexpressing the hAPP695swe (APP) and presenilin-1M146V (PS1) mutations, respectively, were generated at GlaxoSmithKline by standard techniques as previously described (Howlett et al., 2004). In brief, a Thy-1–APP transgene was generated by inserting the 695 aa isoform of human cDNA (APP695) harboring the Swedish double familial mutation (K670N; M671L) into a vector containing the murine Thy-1 gene. The Thy-1–PS-1 transgene was generated by inserting the coding sequence of human PS-1 cDNA harboring the M146V familial mutation into a vector containing the murine Thy-1 gene. Transgenic lines were generated by pronuclear microinjection into fertilized oocytes from either C57BL/6xC3H mice in the case of Thy-1-APP transgene, or into fertilized oocytes from pure C57BL/6 mice in the case of Thy-1–PS-1 transgene. Thy-1 APPswe mice were generated and backcrossed onto a pure C57BL/6 background before crossing with TPM (PS-1 M146V) mice to produce heterozygote double mutant mice. *ASM*$^{+/-}$ mice (C57BL/6 background; Horinouchi et al., 1995) were bred with APP/PS1 mice to generate APP/PS1/*ASM*$^{+/-}$ mice. Because APP/PS1 mice show sex difference in disease progression, we used only male mice. Data analysis of APP/PS1 mice was done at 5 or 9 mo old. Block randomization method was used to allocate the animals to experimental groups. To eliminate the bias, we were blinded in experimental progress such as data collection and data analysis. SCID Beige mice (Charles River) were used for teratoma formation assay. Mice were housed at a 12 h day/12 h night cycle with free access to tap water and food pellets. Mouse studies were approved by the Kyungpook National University Institutional Animal Care and Use Committee (IACUC).

Plasma collection. Human plasma samples were obtained from individuals with AD, PD, and age-matched, non-AD controls from Yonsei University Severance Hospital (Table S1). Informed consent was obtained from all subjects according to the ethics committee guidelines at the Yonsei University Severance Hospital.

Cell culture. Human fibroblast lines (normal, PS1, ApoE4, and PD) acquired from the Coriell Institute were maintained in DMEM with 15% FBS. The human cortical neuronal cell line HCN-2 was acquired from ATCC. Cells with a passage number 10–15 were used in this study. To obtain CM containing ASM, 5×10^5 Chinese hamster ovary cells overexpressing human ASM (He et al., 1999) were cultured in DMEM for 2 d. Cells were washed with PBS and changed with new media. 24 h later, the CM was collected, centrifuged, and filtered using a 0.22 µm filter. We isolated WT, APP/PS1, APP/PS1/*ASM*$^{+/-}$, and *ASM*$^{+/-}$ mouse tail fibroblasts as previously described (Takahashi et al., 2007a) from 9-mo-old mice. For some experiments, cells were treated with purified, recombinant ASM or ASM siRNA to measure autophagy regulation. NH_4Cl was used to inhibit the autophagic flux. For the inhibition of lysosomal ASM uptake, 10 mM M6P or M6P receptor siRNA were added to the fibroblast culture media at the same time as ASM.

Drug or CM treatments. 4-mo-old APP/PS1 mice received 100 µg/g body weight AMI (Sigma-Aldrich) per os in their drinking water for 4 mo, and a control group received water without drug. 3-mo-old C57BL/6 mice were treated with ASM-CM via i.v. (100 µl) or i.c. (3 µl) injections on 10 consecutive days.

Immunofluorescence. Thioflavin S staining was done according to previously described procedures (Lee et al., 2012). We used anti-20G10 (mouse, 1:1,000, provided by D.R. Howlett, GlaxoSmithKline, Harlow, Essex, UK) for Aβ 42, anti-G30 (rabbit, 1:1,000, provided by D.R. Howlett) for Aβ40, rabbit anti–Iba-1 (1:500; Wako), rabbit anti-GFAP (1:500, Dako), mouse anti–α-SMA (1:400; Sigma-Aldrich), rabbit anti-AT8 (1:500; Thermo Fisher Scientific), and rabbit anti–active caspase3 (1:50; EMD Millipore). The sections were analyzed with a laser-scanning confocal microscope (FV1000; Olympus) or with a BX51 microscope (Olympus). MetaMorph software (Molecular Devices) was used to quantification.

Aβ ELISA. For measurement of Aβ40 and Aβ42, we used commercially available ELISA kits (BioSource). Hemispheres of mice were homogenized in buffer containing 0.02M guanidine. ELISA was then performed for Aβ40 and Aβ42 according to the manufacturer's instructions.

Behavioral studies. We performed behavioral studies to assess spatial learning and memory in the Morris water maze as previously described (Lee et al., 2012). Animals were given four trials per day for 10 d to learn the task. At 11 d, animals were given a probe trial in which the platform was removed. Fear conditioning was conducted as previously described techniques (Kojima et al., 2005). On the conditioning day, mice were individually placed into the conditioning chamber. After a 60-s exploratory period, a tone (10 kHz, 70 dB) was delivered for 10 s; this served as the conditioned stimulus (CS). The CS co-terminated with the unconditioned stimulus (US), a scrambled electrical footshock (0.3 mA, 1 s). The CS-US pairing was delivered twice at a 20-s intertrial interval. On day 2, each mouse was placed in the fear-conditioning chamber containing the same exact context, but with no administration of a CS or foot shock. Freezing was analyzed for 5 min. On day 3, a mouse was placed in a test chamber that was different from the conditioning chamber. After a 60-s exploratory period, the tone was presented for 60 s without the footshock. The rate of freezing response of mice was used to measure the fear memory.

Quantitative real-time PCR. RNA was extracted from the brain homogenates and cell lysates using the RNeasy Lipid Tissue Mini kit and RNeasy Plus Mini kit (QIAGEN) according to the manufacturer's instructions. cDNA was synthesized from 5 µg of total RNA using a commercially available kit (Takara Bio Inc.). Quantitative real-time PCR was performed using a Corbett research RG-6000 real-time PCR instrument. Used primers are described in Table S2.

EM. Brain tissues and cells were fixed in 3% glutaraldehyde/0.1 M phosphate buffer, pH 7.4, and postfixed in 1% osmium tetroxide in Sorensen's phosphate buffer. After dehydration in ethyl alcohol, the tissue and cells were embedded in epon (Electron Microscopy Sciences). Samples were cut serially and placed on copper grids and analyzed using a transmission EM (Tecnai). Images were captured on a digital camera and Xplore3D tomography software.

Intracellular protein degradation measurement. Total protein degradation in cultured cells was measured by pulse-chase experiments with 48 h pulse with 2 µCi/ml [^{3}H]-leucine for 48 h to preferentially label long-lived proteins (Lee et al., 2010b).

Western blotting. Samples were immunoblotted as previously described (Settembre et al., 2011; Lee et al., 2012). Primary antibodies to the following

proteins were used: BACE-1 (mouse, 1:1,000; Millipore), LC3 (rabbit, 1:1,000; Cell Signaling Technology), Beclin-1 (rabbit, 1:1,000; Cell Signaling Technology), p62 (rabbit, 1:1,000; Cell Signaling Technology), rab5 (rabbit, 1:1,000; Cell Signaling Technology), rab7 (rabbit, 1:1,000; Cell Signaling Technology), TFEB (rabbit, 1:1,000; Cell Signaling Technology), Lamp1 (rabbit, 1:1,000; Abcam), TFEB (rabbit, 1:500; Novus Biologicals), cathepsin D (goat, 1:500; R&D Systems), 6E10 (mouse, 1:500; Signet), Histon H3 (rabbit, 1:1,000; Cell Signaling Technology), and β-actin (1:1,000; Santa Cruz Biotechnology, Inc.). We performed densitometric quantification using the ImageJ software (National Institutes of Health).

ASM and AC activity assays. We performed the measurements as previously described methods using a UPLC system (Waters; He et al., 2010).

Lipid extraction and ceramide/sphingomyelin quantification. We prepared samples for lipid extraction as previously described (Lee et al., 2010a). To quantify the sphingomyelin and ceramide levels, the dried lipid extract was resuspended in 0.2% Igepal CA-630 (Sigma-Aldrich) and the levels of each lipid were determined using the UPLC system.

Isolation of neuron and microglia. We isolated neuron and microglia from the mouse brain as previously described (Brewer and Torricelli, 2007). In brief, 9-mo-old mice cerebrum were minced in HibernateA (Brainbits LLC)/B27 (Invitrogen) medium and dissociated using papain solution. After tissue trituration, cells were separated by density gradient centrifugation. Fractionated cells were used for ASM activity assay.

LysoTracker labeling and quantification. LysoTracker red (Invitrogen) was used at a final concentration of 75 nM. The cells were trypsinized, resuspended in PBS, and analyzed on a FACSCalibur using FACSDiva software (BD).

Cell viability assays. Cell viability was quantified by using MTT (3-(4,5-Dimethylthiazol-2-yl)-2,5-diphenyltetrazoliumbromide; Sigma-Aldrich) reagent. In brief, human fibroblast was seeded onto 96-well plates at a density of 1.5×10^3 cells per well. 10 μM ASM was added to the culture media, and the cells were incubated for 24 h. MTT stock solution (5 mg/ml) was prepared in PBS (Gibco) and added to the culture media at a final concentration of 1 mg/ml. After 90 min incubation, the media was removed, and the chromogen in the cells was dissolved in DMSO containing 0.01 N NaOH. The absorbance was measured at 570 nm using a 96-well microplate spectrophotometer.

Measurement of activity of cathepsin D. Enzyme activity of cathepsin D was determined with cathepsin D activity fluorometric assay kit according to the manufacturer's protocol (Abcam).

Generation of iPSCs. PS1-iPSCs were established from the PS1 patient's skin fibroblasts (Coriell Institute) as previously described (Okita et al., 2007), with slight modifications. In brief, PS1 fibroblasts were seeded at 3×10^5 cells in 60 mm^2 dishes coated with gelatin. On day 1, the VSV-G pseudotyped retroviral vector system carrying OCT4, SOX2, KLF4, and c-Myc was added to fibroblast cultures. On day 2, cells were subjected to the same transduction procedures and harvested 24 h later. Transduced cells were replated on mouse embryonic fibroblast (MEF) layers in 100 mm^2 dishes containing the fibroblast medium. On the next day, the medium was changed to complete ES medium with 0.5 mM valproic acid (Sigma-Aldrich), and thereafter changed every other day. After 20 d, ES-like colonies appeared and were picked up to be reseeded on new MEF feeder cells. Cloned ES-like colonies were subjected to further analysis. Normal iPSC line (HPS0063) was obtained from the RIKEN Bioresource Center (Takahashi et al., 2007b).

In vitro differentiation of human iPSCs. Neural differentiation of iPSCs was performed as described previously (Okada et al., 2008). iPSC colonies were detached from feeder layers and cultured in suspension as embryonic body for ∼30 d in bacteriological dishes. Embryonic bodies were then enzymatically dissociated into single cells and the dissociated cells cultured in suspension in serum-free media hormone mix media (Okada et al., 2008) for 10–14 d to allow the formation of neurospheres. Neurospheres were passaged repeatedly by dissociation into single cells followed by culture in the same manner. Typically, neurospheres between passages 3 and 8 were used for analysis. For terminal differentiation, dissociated neurospheres were allowed to adhere to poly-L-ornithine– and laminin-coated coverslips and cultured for 10 d.

AP, senescence-associated-β-galactosidase (SA-β-gal), and immunocytochemical staining. AP staining was performed using an ES-AP detection kit (EMD Millipore) according to manufacturer's recommendations. SA-β-gal activity was detected using SA-β-gal staining kit (Cell Signaling Technology) according to manufacturer's protocol. For immunocytochemical analysis, we used anti-SSEA4, TRA-1-60, TRA-1-81 (mouse, 1:100; EMD Millipore), anti–β-III-tubulin (mouse, 1:400; EMD Millipore), rabbit anti–LC-3B (1:200; Cell Signaling Technology), rabbit anti-ASM (1:1,000, Abcam), mouse anti-LAMP1 (1:100; Abcam), and mouse anti-LBPA (1:500; Echelon).

Teratoma formation and histological analysis. Established iPSCs were prepared at 10^7 cells/ml in PBS. Suspended cells ($1–3 \times 10^6$) were injected into testes of anesthetized male SCID Beige mice. 8 wk after transplantation, mice were sacrificed and tumors were dissected. Tumor samples were fixed in 10% formalin and embedded in paraffin. Sections were stained with hematoxylin and eosin.

Statistical analysis. Comparisons between two groups were performed with Student's *t* test. In cases where more than two groups were compared with each other, a one-way analysis of variance (ANOVA) was used, followed by Tukey's HSD test. All statistical analysis was performed using SPSS statistical software. $P < 0.05$ was considered to be significant.

Online supplemental material. Table S1 shows subjects' characteristics. Table S2 shows sequences of primer pairs. Online supplemental material is available at http://www.jem.org/cgi/content/full/jem.20132451/DC1.

This work was supported by the Bio & Medical Technology Development Program (2010-0020234, 2011-0019356, 2012M3A9C6049913, and 2012M3A9C6050107) of the National Research Foundation (NRF) of Korea funded by the Ministry of Science, ICT & Future Planning, Republic of Korea.

The authors declare no competing financial interests.

Author contributions: J.K. Lee, H.K. Jin, M.H. Park, B.R. Kim, P.H. Lee, H. Nakauchi, J.E. Carter, and X. He performed experiments and analyzed data, J.K. Lee, H.K. Jin, and J.S. Bae designed the study and wrote the paper. E.H. Schuchman and J.S. Bae interpreted the data and reviewed the paper. All authors discussed results and commented on the manuscript.

Submitted: 26 November 2013
Accepted: 20 June 2014

REFERENCES

Boland, B., A. Kumar, S. Lee, F.M. Platt, J. Wegiel, W.H. Yu, and R.A. Nixon. 2008. Autophagy induction and autophagosome clearance in neurons: relationship to autophagic pathology in Alzheimer's disease. *J. Neurosci.* 28:6926–6937. http://dx.doi.org/10.1523/JNEUROSCI.0800-08.2008

Brewer, G.J., and J.R. Torricelli. 2007. Isolation and culture of adult neurons and neurospheres. *Nat. Protoc.* 2:1490–1498. http://dx.doi.org/10.1038/nprot.2007.207

Cataldo, A.M., C.M. Peterhoff, S.D. Schmidt, N.B. Terio, K. Duff, M. Beard, P.M. Mathews, and R.A. Nixon. 2004. Presenilin mutations in familial Alzheimer disease and transgenic mouse models accelerate neuronal lysosomal pathology. *J. Neuropathol. Exp. Neurol.* 63:821–830.

Cuervo, A.M., L. Stefanis, R. Fredenburg, P.T. Lansbury, and D. Sulzer. 2004. Impaired degradation of mutant alpha-synuclein by chaperone-mediated autophagy. *Science.* 305:1292–1295. http://dx.doi.org/10.1126/science.1101738

Cutler, R.G., J. Kelly, K. Storie, W.A. Pedersen, A. Tammara, K. Hatanpaa, J.C. Troncoso, and M.P. Mattson. 2004. Involvement of oxidative

stress-induced abnormalities in ceramide and cholesterol metabolism in brain aging and Alzheimer's disease. *Proc. Natl. Acad. Sci. USA.* 101:2070–2075. http://dx.doi.org/10.1073/pnas.0305799101

Dhami, R., and E.H. Schuchman. 2004. Mannose 6-phosphate receptor-mediated uptake is defective in acid sphingomyelinase-deficient macrophages: implications for Niemann-Pick disease enzyme replacement therapy. *J. Biol. Chem.* 279:1526–1532. http://dx.doi.org/10.1074/jbc.M309465200

Di Paolo, G., and T.W. Kim. 2011. Linking lipids to Alzheimer's disease: cholesterol and beyond. *Nat. Rev. Neurosci.* 12:284–296. http://dx.doi.org/10.1038/nrn3012

Ginsberg, S.D., E.J. Mufson, S.E. Counts, J. Wuu, M.J. Alldred, R.A. Nixon, and S. Che. 2010. Regional selectivity of rab5 and rab7 protein upregulation in mild cognitive impairment and Alzheimer's disease. *J. Alzheimers Dis.* 22:631–639.

Górska, M., E. Barańczuk, and A. Dobrzyń. 2003. Secretory Zn^{2+}-dependent sphingomyelinase activity in the serum of patients with type 2 diabetes is elevated. *Horm. Metab. Res.* 35:506–507. http://dx.doi.org/10.1055/s-2003-41810

Grimm, M.O., H.S. Grimm, A.J. Pätzold, E.G. Zinser, R. Halonen, M. Duering, J.A. Tschäpe, B. De Strooper, U. Müller, J. Shen, and T. Hartmann. 2005. Regulation of cholesterol and sphingomyelin metabolism by amyloid-β and presenilin. *Nat. Cell Biol.* 7:1118–1123. http://dx.doi.org/10.1038/ncb1313

Grösgen, S., M.O. Grimm, P. Friess, and T. Hartmann. 2010. Role of amyloid beta in lipid homeostasis. *Biochim. Biophys. Acta.* 1801:966–974. http://dx.doi.org/10.1016/j.bbalip.2010.05.002

Hartmann, T., J. Kuchenbecker, and M.O. Grimm. 2007. Alzheimer's disease: the lipid connection. *J. Neurochem.* 103:159–170. http://dx.doi.org/10.1111/j.1471-4159.2007.04715.x

Haughey, N.J., V.V. Bandaru, M. Bae, and M.P. Mattson. 2010. Roles for dysfunctional sphingolipid metabolism in Alzheimer's disease neuropathogenesis. *Biochim. Biophys. Acta.* 1801:878–886. http://dx.doi.org/10.1016/j.bbalip.2010.05.003

He, X., and E.H. Schuchman. 2012. Potential role of acid sphingomyelinase in environmental health. *Zhong Nan Da Xue Xue Bao Yi Xue Ban.* 37:109–125.

He, X., S.R. Miranda, X. Xiong, A. Dagan, S. Gatt, and E.H. Schuchman. 1999. Characterization of human acid sphingomyelinase purified from the media of overexpressing Chinese hamster ovary cells. *Biochim. Biophys. Acta.* 1432:251–264. http://dx.doi.org/10.1016/S0167-4838(99)00069-2

He, X., Y. Huang, B. Li, C.X. Gong, and E.H. Schuchman. 2010. Deregulation of sphingolipid metabolism in Alzheimer's disease. *Neurobiol. Aging.* 31:398–408. http://dx.doi.org/10.1016/j.neurobiolaging.2008.05.010

Horinouchi, K., S. Erlich, D.P. Perl, K. Ferlinz, C.L. Bisgaier, K. Sandhoff, R.J. Desnick, C.L. Stewart, and E.H. Schuchman. 1995. Acid sphingomyelinase deficient mice: a model of types A and B Niemann-Pick disease. *Nat. Genet.* 10:288–293. http://dx.doi.org/10.1038/ng0795-288

Howlett, D.R., J.C. Richardson, A. Austin, A.A. Parsons, S.T. Bate, D.C. Davies, and M.I. Gonzalez. 2004. Cognitive correlates of Aβ deposition in male and female mice bearing amyloid precursor protein and presenilin-1 mutant transgenes. *Brain Res.* 1017:130–136. http://dx.doi.org/10.1016/j.brainres.2004.05.029

Jenkins, R.W., D. Canals, and Y.A. Hannun. 2009. Roles and regulation of secretory and lysosomal acid sphingomyelinase. *Cell. Signal.* 21:836–846. http://dx.doi.org/10.1016/j.cellsig.2009.01.026

Katsel, P., C. Li, and V. Haroutunian. 2007. Gene expression alterations in the sphingolipid metabolism pathways during progression of dementia and Alzheimer's disease: a shift toward ceramide accumulation at the earliest recognizable stages of Alzheimer's disease? *Neurochem. Res.* 32:845–856. http://dx.doi.org/10.1007/s11064-007-9297-x

Kirkegaard, T., A.G. Roth, N.H. Petersen, A.K. Mahalka, O.D. Olsen, I. Moilanen, A. Zylicz, J. Knudsen, K. Sandhoff, C. Arenz, et al. 2010. Hsp70 stabilizes lysosomes and reverts Niemann-Pick disease-associated lysosomal pathology. *Nature.* 463:549–553. http://dx.doi.org/10.1038/nature08710

Kojima, N., T. Sakamoto, S. Endo, and H. Niki. 2005. Impairment of conditioned freezing to tone, but not to context, in Fyn-transgenic mice: relationship to NMDA receptor subunit 2B function. *Eur. J. Neurosci.* 21:1359–1369. http://dx.doi.org/10.1111/j.1460-9568.2005.03955.x

Kondo, T., M. Asai, K. Tsukita, Y. Kutoku, Y. Ohsawa, Y. Sunada, K. Imamura, N. Egawa, N. Yahata, K. Okita, et al. 2013. Modeling Alzheimer's disease with iPSCs reveals stress phenotypes associated with intracellular Aβ and differential drug responsiveness. *Cell Stem Cell.* 12:487–496. http://dx.doi.org/10.1016/j.stem.2013.01.009

Lahiri, S., and A.H. Futerman. 2007. The metabolism and function of sphingolipids and glycosphingolipids. *Cell. Mol. Life Sci.* 64:2270–2284. http://dx.doi.org/10.1007/s00018-007-7076-0

Lai, A.Y., and J. McLaurin. 2012. Inhibition of amyloid-beta peptide aggregation rescues the autophagic deficits in the TgCRND8 mouse model of Alzheimer disease. *Biochim. Biophys. Acta.* 1822:1629–1637. http://dx.doi.org/10.1016/j.bbadis.2012.07.003

Lang, P.A., M. Schenck, J.P. Nicolay, J.U. Becker, D.S. Kempe, A. Lupescu, S. Koka, K. Eisele, B.A. Klarl, H. Rübben, et al. 2007. Liver cell death and anemia in Wilson disease involve acid sphingomyelinase and ceramide. *Nat. Med.* 13:164–170. http://dx.doi.org/10.1038/nm1539

Lee, H., J.K. Lee, W.K. Min, J.H. Bae, X. He, E.H. Schuchman, J.S. Bae, and H.K. Jin. 2010a. Bone marrow-derived mesenchymal stem cells prevent the loss of Niemann-Pick type C mouse Purkinje neurons by correcting sphingolipid metabolism and increasing sphingosine-1-phosphate. *Stem Cells.* 28:821–831. http://dx.doi.org/10.1002/stem.401

Lee, J.H., W.H. Yu, A. Kumar, S. Lee, P.S. Mohan, C.M. Peterhoff, D.M. Wolfe, M. Martinez-Vicente, A.C. Massey, G. Sovak, et al. 2010b. Lysosomal proteolysis and autophagy require presenilin 1 and are disrupted by Alzheimer-related PS1 mutations. *Cell.* 141:1146–1158. http://dx.doi.org/10.1016/j.cell.2010.05.008

Lee, J.K., E.H. Schuchman, H.K. Jin, and J.S. Bae. 2012. Soluble CCL5 derived from bone marrow-derived mesenchymal stem cells and activated by amyloid β ameliorates Alzheimer's disease in mice by recruiting bone marrow-induced microglia immune responses. *Stem Cells.* 30:1544–1555. http://dx.doi.org/10.1002/stem.1125

Li, J., T. Kanekiyo, M. Shinohara, Y. Zhang, M.J. LaDu, H. Xu, and G. Bu. 2012. Differential regulation of amyloid-β endocytic trafficking and lysosomal degradation by apolipoprotein E isoforms. *J. Biol. Chem.* 287:44593–44601. http://dx.doi.org/10.1074/jbc.M112.420224

Mielke, M.M., and C.G. Lyketsos. 2010. Alterations of the sphingolipid pathway in Alzheimer's disease: new biomarkers and treatment targets? *Neuromolecular Med.* 12:331–340. http://dx.doi.org/10.1007/s12017-010-8121-y

Mielke, M.M., V.V. Bandaru, N.J. Haughey, J. Xia, L.P. Fried, S. Yasar, M. Albert, V. Varma, G. Harris, E.B. Schneider, et al. 2012. Serum ceramides increase the risk of Alzheimer disease: the Women's Health and Aging Study II. *Neurology.* 79:633–641. http://dx.doi.org/10.1212/WNL.0b013e318264e380

Nixon, R.A. 2007. Autophagy, amyloidogenesis and Alzheimer disease. *J. Cell Sci.* 120:4081–4091. http://dx.doi.org/10.1242/jcs.019265

Nixon, R.A., and D.S. Yang. 2011. Autophagy failure in Alzheimer's disease—locating the primary defect. *Neurobiol. Dis.* 43:38–45. http://dx.doi.org/10.1016/j.nbd.2011.01.021

Okada, Y., A. Matsumoto, T. Shimazaki, R. Enoki, A. Koizumi, S. Ishii, Y. Itoyama, G. Sobue, and H. Okano. 2008. Spatiotemporal recapitulation of central nervous system development by murine embryonic stem cell-derived neural stem/progenitor cells. *Stem Cells.* 26:3086–3098. http://dx.doi.org/10.1634/stemcells.2008-0293

Okita, K., T. Ichisaka, and S. Yamanaka. 2007. Generation of germline-competent induced pluripotent stem cells. *Nature.* 448:313–317. http://dx.doi.org/10.1038/nature05934

Petrache, I., V. Natarajan, L. Zhen, T.R. Medler, A.T. Richter, C. Cho, W.C. Hubbard, E.V. Berdyshev, and R.M. Tuder. 2005. Ceramide upregulation causes pulmonary cell apoptosis and emphysema-like disease in mice. *Nat. Med.* 11:491–498. http://dx.doi.org/10.1038/nm1238

Rubinsztein, D.C., A.M. Cuervo, B. Ravikumar, S. Sarkar, V. Korolchuk, S. Kaushik, and D.J. Klionsky. 2009. In search of an "autophagomometer". *Autophagy.* 5:585–589. http://dx.doi.org/10.4161/auto.5.5.8823

Santana, P., L.A. Peña, A. Haimovitz-Friedman, S. Martin, D. Green, M. McLoughlin, C. Cordon-Cardo, E.H. Schuchman, Z. Fuks, and R. Kolesnick. 1996. Acid sphingomyelinase-deficient human lymphoblasts and mice are defective in radiation-induced apoptosis. *Cell.* 86:189–199. http://dx.doi.org/10.1016/S0092-8674(00)80091-4

Selkoe, D.J. 2001. Alzheimer's disease: genes, proteins, and therapy. *Physiol. Rev.* 81:741–766.

Sentelle, R.D., C.E. Senkal, W. Jiang, S. Ponnusamy, S. Gencer, S.P. Selvam, V.K. Ramshesh, Y.K. Peterson, J.J. Lemasters, Z.M. Szulc, et al. 2012. Ceramide targets autophagosomes to mitochondria and induces lethal mitophagy. *Nat. Chem. Biol.* 8:831–838. http://dx.doi.org/10.1038/nchembio.1059

Settembre, C., C. Di Malta, V.A. Polito, M. Garcia Arencibia, F. Vetrini, S. Erdin, S.U. Erdin, T. Huynh, D. Medina, P. Colella, et al. 2011. TFEB links autophagy to lysosomal biogenesis. *Science*. 332:1429–1433. http://dx.doi.org/10.1126/science.1204592

Smith, E.L., and E.H. Schuchman. 2008. The unexpected role of acid sphingomyelinase in cell death and the pathophysiology of common diseases. *FASEB J.* 22:3419–3431. http://dx.doi.org/10.1096/fj.08-108043

Su, H., F. Li, M.J. Ranek, N. Wei, and X. Wang. 2011. COP9 signalosome regulates autophagosome maturation. *Circulation*. 124:2117–2128. http://dx.doi.org/10.1161/CIRCULATIONAHA.111.048934

Takahashi, K., K. Okita, M. Nakagawa, and S. Yamanaka. 2007a. Induction of pluripotent stem cells from fibroblast cultures. *Nat. Protoc.* 2:3081–3089. http://dx.doi.org/10.1038/nprot.2007.418

Takahashi, K., K. Tanabe, M. Ohnuki, M. Narita, T. Ichisaka, K. Tomoda, and S. Yamanaka. 2007b. Induction of pluripotent stem cells from adult human fibroblasts by defined factors. *Cell*. 131:861–872. http://dx.doi.org/10.1016/j.cell.2007.11.019

Tamboli, I.Y., H. Hampel, N.T. Tien, K. Tolksdorf, B. Breiden, P.M. Mathews, P. Saftig, K. Sandhoff, and J. Walter. 2011. Sphingolipid storage affects autophagic metabolism of the amyloid precursor protein and promotes Aβ generation. *J. Neurosci.* 31:1837–1849. http://dx.doi.org/10.1523/JNEUROSCI.2954-10.2011

Teichgräber, V., M. Ulrich, N. Endlich, J. Riethmüller, B. Wilker, C.C. De Oliveira-Munding, A.M. van Heeckeren, M.L. Barr, G. von Kürthy, K.W. Schmid, et al. 2008. Ceramide accumulation mediates inflammation, cell death and infection susceptibility in cystic fibrosis. *Nat. Med.* 14:382–391. http://dx.doi.org/10.1038/nm1748

Wymann, M.P., and R. Schneiter. 2008. Lipid signalling in disease. *Nat. Rev. Mol. Cell Biol.* 9:162–176. http://dx.doi.org/10.1038/nrm2335

Yankner, B.A., T. Lu, and P. Loerch. 2008. The aging brain. *Annu. Rev. Pathol.* 3:41–66. http://dx.doi.org/10.1146/annurev.pathmechdis.2.010506.092044

Yu, W.H., A.M. Cuervo, A. Kumar, C.M. Peterhoff, S.D. Schmidt, J.H. Lee, P.S. Mohan, M. Mercken, M.R. Farmery, L.O. Tjernberg, et al. 2005. Macroautophagy—a novel β-amyloid peptide-generating pathway activated in Alzheimer's disease. *J. Cell Biol.* 171:87–98. http://dx.doi.org/10.1083/jcb.200505082

Zeng, X., J.H. Overmeyer, and W.A. Maltese. 2006. Functional specificity of the mammalian Beclin-Vps34 PI 3-kinase complex in macroautophagy versus endocytosis and lysosomal enzyme trafficking. *J. Cell Sci.* 119:259–270. http://dx.doi.org/10.1242/jcs.02735

Zhou, J.W., X.R. Cheng, J.P. Cheng, W.X. Zhou, and Y.X. Zhang. 2012. The activity and mRNA expression of β-secretase, cathepsin D, and cathepsin B in the brain of senescence-accelerated mouse. *J. Alzheimers Dis.* 28:471–480.